

1. - CAT - 44

IN -

43739

DOE/JPL-956046/86-1
9950-1202

RECEIVED

MAR 12 1986

PATENTS AND TU OFFICE

P-65

Cornell University
Department of Materials Science and Engineering
Bard Hall
Ithaca, NY 14853

ELECTRICAL, STRUCTURAL AND CHEMICAL CHARACTERIZATION OF SI SHEET MATERIAL

Annual Report - Contract No. 956046

Principal Investigator: Dieter G. Ast

Covering Period: September 1, 1984 - August 31, 1985

"The JPL Flat Plate Solar Array Project is sponsored by the U.S. Department of Energy and forms part of the Solar Photovoltaic Conversion Program to initiate a major effort toward the development of flat plate solar arrays. This work was performed for the Jet Propulsion Laboratory, California Institute of Technology by agreement between NASA and DOE."

(NASA-CR-179949) ELECTRICAL, STRUCTURAL AND
CHEMICAL CHARACTERIZATION OF Si SHEET
MATERIAL Annual Report, 1 Sep. 1984 - 31
Aug. 1985 (Cornell Univ.) 65 p CSDL 10A

N87-13855

Unclas
G3/44 43635

ABSTRACT

Study of Web Dendritic Si ribbons under four-point bending stress was undertaken to lead to an understanding of how Web Si deforms under a well-defined applied stress. Since the mechanical properties of Si are known to depend on the O content of the material, O measurements using Fourier Transform Infrared Spectroscopy were done to determine a proper control sample of non-defected single crystal Si.

Four point bending revealed a unique two step bending behavior for the Web Si ribbons. An initial theory for this behavior involves the interaction of the dislocations generated by the deformation with the central twin planes of the ribbons. O measurements showed a uniformly high O content for the Web Si ribbons, approximately 10^{18} atoms/cm³ for all the samples measured. All the Web samples had a much broader absorption peak at 9 μ m than is usually seen for well-annealed single crystal Si. This broadening is thought to be related to stress in the Web Si ribbons. Two samples containing a known amount of residual stress support this hypothesis. Also, a shoulder on the infrared absorption peak associated with interstitial O in Si appears in the transmission vs. wavenumber plots for some of the Web samples. In the literature, this shoulder has been associated with O-vacancy complexes or with O at dislocations. The O content and configuration do not seem to correlate with the growth configuration of the Web Si ribbon.

ACKNOWLEDGEMENTS

We wish to thank Dr. J. Kalejs and Mr. A. Menna at Mobil Solar Energy Corporation for the use of their four point bending set-up and for many helpful discussions. We also wish to thank Dr. A. Baghdadi at the National Bureau of Standards for the use of the Fourier Transform Infrared Spectroscope and for his help in interpretation of our data.

"This report was prepared as an account of work sponsored by the United States Government. Neither the United States nor the U.S. Department of Energy, nor any of their employees, nor any of their contractors, subcontractors, of their employees, makes any warranty express or implied, or assumes any legal liability or responsibility for the accuracy, completeness or usefulness of any information, apparatus, product or process disclosed, or represents that its use would not infringe privately owned rights."

Table of Contents

List of Figures	page 2
Introduction	page 4
Four Point Bending of Web Silicon Ribbons	page 7
Oxygen Measurements in Web Silicon Ribbons	page 20
Surface Profiles of Web Silicon Ribbons	page 32
Conclusions	page 36
References	page 39

Figures

- Figure 1: Schematic of Four-Point Bending Set-Up.
- Figure 2: Four-Point Bending Data for Web Samples J372-1.5 and J372-2.4, and a Float Zone Sample.
- Figure 3: Four-Point Bending Data for Web Sample Z071-7.3.
- Figure 4: Four-Point Bending Data for Web Sample N140-10.3.
- Figure 5: Four-Point Bending Data for Web Sample R485-7.5-1.
- Figure 6: Four-Point Bending Data for Web Sample R485-7.5-2.
- Figure 7: IR Transmission vs. Wavenumber for Web Sample J376-4.3.
- Figure 8: IR Transmission vs. Wavenumber for Web Sample J376-4.3.
- Figure 9: IR Transmission vs. Wavenumber for a Cz Sample.
- Figure 10: IR Transmission vs. Wavenumber for Various Heat Treatments (Courtesy: I. Koguchi)
- Figure 11: Separation of Two Peaks Seen in Figure 8.
- Figure 12: IR Transmission vs. Wavenumber for Web Sample N128-19.1, Grown in Z058 Configuration.
- Figure 13: IR Transmission vs. Wavenumber for Web Samples 2284-15.8 and 2-305-5.11, Grown in the J435 Configuration.
- Figure 14: IR Transmission vs. Wavenumber for Web Sample R479-13.2, Grown in the J460 Configuration.
- Figure 15: IR Transmission vs. Wavenumber for Web Sample R479-13.2, Before and After an HF Clean.
- Figure 16: IR Transmission vs. Wavenumber for Two Areas along Web Sample N128-19.1.
- Figure 17: IR Transmission vs. Wavenumber for Three Areas across the Width of Web Sample Z025-3.7A.
- Figure 18: IR Transmission vs. Wavenumber for Two Web Samples with a Known Amount of Residual Stress.

Figure 19: Surface Profile of Web Sample J376-4.3.

Figure 20: Surface Profile of Web Sample J376-4.3.

Figure 21: Surface Profile of Web Sample RE343-3.3.

Figure 22: Expanded Surface Profile of Web Sample RE343-3.3.

Introduction

During the reporting period of September, 1984 to August, 1985, we studied the deformation behavior of Dendritic Web Ribbon silicon under four point bending stress. Four-point bending experiments were carried out at Mobil Solar Energy Corporation on samples supplied by JPL.

Dendritic Web silicon has a unique crystalline structure. The ribbon is a single crystal but its mid-plane contains one or several closely spaced twin planes parallel to the ribbon surface[1]. In addition, Web material contains bulk dislocations, some of which appear at the ribbon surface. Surface etching shows a high dislocation density at the ribbon center and near the dendrites, separated by regions of low dislocation density. Angle lapping and etching reveals dislocations at the twin plane, probably trapped there as a result of stress during ribbon growth [2]. The stresses experienced during ribbon growth are not well understood, but the plastic deformation as a result of these stresses in the form of dislocations intersecting the ribbon surface and dislocations trapped at the twin planes can be studied in an attempt to understand the stresses generated during the crystal growth. In addition, elastic residual stresses are present which can lead to lower mobility for

minority carriers and, consequently, to lower efficiencies in finished solar cells, and can also limit the rate at which the silicon ribbons can be grown. It has become clear that an understanding of the growth-rate and efficiency limiting stresses must be attained to optimize the growth of Dendritic Web silicon.

For this reason, we studied the behavior of Web silicon under four-point bending, because understanding of how Web silicon deforms under a well-defined applied stress can lead to a model of the stresses experienced during ribbon growth.

Previous work on Edge-Defined Film-Fed Growth (EFG) ribbons under this Contract has determined that twins in the material interfere with the motions of dislocations [3]. This interference should lead to differences in the creep behavior of the Web material and an untwinned single crystal of identical dimensions. And indeed, our experiments have shown that Web silicon deforms very differently from single crystal silicon, either Float-Zone or Czochralski, and from polycrystalline material such as EFG silicon. In fact, Web silicon has shown a unique two-stage deformation behavior. The mechanisms responsible for these two stages are not clear and further study is needed to relate this behavior to the ribbon growth conditions and quality.

Since oxygen hardens the silicon lattice, the amount of oxygen and the way the oxygen is bound in the silicon lattice is a major factor in the behavior of silicon under stress [4]. As shown in the following section, Web silicon contains nearly the maximum amount of oxygen soluble in silicon at the growth temperature. Part of the oxygen appears in the infrared absorption peak associated with oxygen in interstitial sites (Si-O-Si) in the silicon lattice,

and part of the oxygen appears in an infrared absorption line that forms a shoulder on the standard interstitial oxygen peak. Various interpretations of this shoulder have been given in the literature, and the peak has been ascribed variously to homogeneously distributed precipitates of the coesite phase of SiO_2 in the bulk [5], to oxygen segregated to dislocation cores where, according to Bourret, it forms a coesite-like arrangement [6], or to oxygen involved in a complex with silicon interstitials and vacancies [7]. In the case of as-grown Web silicon, we believe that the coesite phase is likely to nucleate heterogeneously at the grown-in dislocations, since dislocations are present in the growing ribbon and heterogeneous nucleation is the preferred nucleation mechanism for any system. Whether oxygen does or does not precipitate on deformation induced dislocations generated in the cool-down phase of ribbon growth ($T < 750^\circ\text{C}$) is an open question. The oxygen decoration of these dislocations will depend critically on the ratio of dislocation mobility to oxygen mobility. Because decorated dislocations, as a rule, are less mobile than undecorated ones, the residual stress will be higher if the oxygen can move sufficiently fast to keep up with the dislocations. If the oxygen is bound to dislocations in the twin planes, the motion of dislocations through the twin planes is likely to be further impeded because the interaction of bulk dislocations with the intrinsic dislocations in the twin planes will be hindered by dislocation pinning at oxygen precipitates. The amount and condition of the oxygen in the Web silicon, and its behavior with temperature and growth conditions, needs to be studied to determine the effect of the oxygen on the growing ribbon and on the solar cells fabricated on these ribbons.

Four-Point Bending of Web Silicon Ribbons

Introduction

To study the effects of stress on Web ribbons, the ribbons had to be stressed in a controlled manner. Tensile testing of silicon is very difficult because the material is brittle at room temperature and it is hard to grip the specimen properly for a tensile test without damage to the specimen. We therefore decided to introduce deformation by bending. There are two possible ways to introduce deformation by bending; three point bending or four point bending. The four point bending is the simplest form of bending to analyze because the sample experiences a constant bending moment between the inner load pins. In three point bending, the moment increases linearly towards the center pin and is therefore not constant over any appreciable area. We decided to creep deform the Web ribbons in four point bending for simplicity in sample preparation and control in sample deformation.

Four-point bending of Web silicon ribbons was carried out on an apparatus at Mobil Solar Energy Corporation (MSEC) with the cooperation of Dr. Juris Kalejs [8]. A schematic diagram of the bending apparatus is shown in Figure

1, showing the location of the sample, the thermocouples, the deflection probe, and the load-applying rollers. The top rollers are separated by about an inch and are fixed, and the bottom rollers are attached to the applied load through a pulley system so that a bending moment is applied to the sample by moving the bottom rollers upward against the sample bottom. The deflection of the sample is determined simply by the downward motion of a deflection probe which rests in the center of the sample. The deflection of the sample center has been shown to agree well with the amount of curvature measured in the sample after cool-down and removal from the bending apparatus. The samples tested were all cut to a length of four inches, but the width of the sample was determined by the width that the particular ribbon was grown.

The samples were brought to the test temperature and a load, W , was applied. The sample was allowed to creep under the applied load and the deflection of the ribbon center was measured with time.

Creep is the general name applied to plastic deformation which occurs under conditions of constant temperature and constant stress, or time-dependent plastic deformation. Creep can occur by a variety of mechanisms [9], including dislocation climb and glide (where the strain rate is proportional to some power of the applied stress, sometimes called power-law creep), and direct vacancy transport (where the strain rate is directly proportional to the applied stress. When the vacancy transport is bulk controlled, the creep is called Nabarro-Herring creep; when controlled by vacancy transport through the grain boundaries it is called Coble creep.) Which mechanism controls the observed creep in a sample depends on the temperature and stress level that the sample experiences during the test.

The stress levels in the Web samples during four-point bending are calculated by simple beam-bending theory [10].

The Web sample can be modeled as a bar of rectangular cross-section, $b \times t$, where b is the width of the ribbon and t is the ribbon thickness. Using standard mechanics, the bending moment, M , applied to the sample is

$$M = \frac{Wa}{2} \quad (\text{gm} \cdot \text{cm})$$

determined by the spacing between the inner and outer pins, a , and the applied weight, W . The stress in the outer fiber of a rectangular cross-section ribbon is

$$\sigma_{\max} = \frac{Mc}{I} \quad (\text{gm} \cdot \text{cm}^{-2})$$

where c/I is a geometrical factor called the inverse section modulus and is given by

$$\frac{c}{I} = \frac{6}{bt^3} \quad (\text{cm}^{-3})$$

The deflection in the center of the ribbon due to the applied weight is given by

$$\delta_{\max} = \frac{[Wa(h-2a)^2]}{16EI}$$

where E is the Young's modulus of the silicon, 1.9×10^{12} dyn/cm² in the [111] direction, and I is the moment of inertia of the rectangular bar. C is the distance from the fiber where the maximum stress occurs (in this case, the ribbon surface) from the neutral stress bending axis. I and c are given by

$$I = \frac{bt^3}{12}$$

$$c = \frac{t}{2}$$

In the system at MSEC

$$h = 5 \text{ cm}$$

$$a = 1.25 \text{ cm}$$

so the relationships become

$$M = 0.625 W$$

$$\delta = 3.08 \times 10^{-12} \frac{W}{bt^3}$$

$$\sigma = 3.75 \frac{W}{bt^2}$$

These elastic solutions are also good for inelastic creep provided that the strain rate is proportional to the first power of the stress. If the sample is deforming by a power law creep then the problem is more complex and

numerical solutions must be applied [11].

Initially, we tried to bend the ribbons at very high temperatures (about 1350°C) to avoid the temperature region where the mechanisms for creep in silicon are controversial (around 900°C). However, because the Web ribbons are thin, they began to creep under the load of the deflection measuring probe (about 7 gm) when the temperature reached about 1180°C. It was decided to test the samples at 1000°C to avoid an uncontrolled "three-point" bending under the weight of the probe, even though this temperature range is undesirable from the standpoint of interpretation of the deformation mechanisms. All ribbon tests reported here were carried out at 1000°C.

One Web ribbon was tested with the dendrites still attached to the ribbon. There was little bending even under a large applied load. We believe that this is a result of the stiffness of the dendrites and not the strength of the actual Web ribbon. The curve of deflection vs. time is shown in Figure 2, and it can be seen that the Web with the dendrites on did not bend appreciably even under twice the load experienced by the single-crystal Float Zone (FZ) sample tested. It appears from this result that the dendrites are a significant help in strengthening the Web ribbons during any kind of handling. All other samples tested had the dendrites removed before testing so that the deflection measured resulted from plastic deformation of the actual Web ribbon and not from the support that the ribbon receives from the dendrites.

Samples obtained from Westinghouse and from JPL were from three growth configurations; J435, generally regarded as producing the ribbons with the highest amount of stress, J460, an improvement on the J435 configuration, and Z058, the growth configuration producing ribbons with little or no measurable

residual stress. Only samples from growth configurations J435 and Z058 were tested. The growth configuration of each sample will be identified in parentheses after the sample number.

Four-Point Bending Results

Sample J372-1.5 was tested with an applied stress of 27 MPa. The resulting deflection vs. time curve is shown in Figure 2. The results for the Web ribbon are obviously very different from the curve obtained from testing the single crystal FZ sample. First, the Web sample is seen to begin to creep as soon as the load is applied. In single crystal material, there is a delay period after the load is applied where dislocations, which are necessary for plastic deformation, are generated. In Web silicon, dislocations are present as a result of the growth, and hence there is no time lag between plastic deformation and loading. In the single crystal FZ material, once the deformation begins, the sample continues to creep at a fairly constant rate until further deflection is no longer measurable in the bending apparatus. One reason that the FZ material creeps at a rapid rate is that the material contains no oxygen, which solute solution hardens the lattice and increases the friction opposing dislocation motion. The Web sample shows initially a high creep rate, but after approximately 1 minute the creep rate decreases to almost zero. Then another period of rapid creep commences, followed by a period of slow creep. This sequence repeats one more time before the test was ended. This unusual fast creep-slow creep behavior is not commonly observed in bending samples and was cause for a great deal of speculation as to the mechanism causing it. Since this behavior was not seen on any sample other than Web silicon tested in this apparatus, we believe that it is not an artifact of the set-up or the measuring devices. Also, other Web samples

tested (to be discussed below) showed indications of the same type of behavior, which supports the idea that the oscillations in the creep rate are related in some way to the structure of the Web silicon ribbons.

The model we are currently considering is that of dislocations initially moving on $\{111\}$ planes inclined 54° to the ribbon surface, starting at the surface, which is the most highly stressed region in the ribbon. When the dislocations move towards the ribbon center, they initially experience a decreasing shear stress. This is so because the initial stress distribution is elastic and the stress increases linearly with the distance from the neutral bending axis. However, after some time the stress will be almost constant throughout the ribbon if power law conditions apply. In this case, a classical dislocation pile-up against the twin plane is formed, resulting in a decrease in the observed deflection rate. When N dislocations in a constant stress field, σ , are piled up at the twin planes, the local stress, σ_1 , generated on the leading dislocation is equal to $N\sigma$. At some stress level, the local stress becomes sufficient to cause the dislocations nearest the twin planes to interact with the twin planes and cause reaction products of this interaction to travel to the opposite surface of the ribbon, resulting in a sudden large amount of deformation. This theory of dislocation punch-through fits all the observations, but much work needs to be done to determine that this is indeed the mechanism causing the two-stage creep behavior. Other ribbons tested showed a similar two-stage creep behavior, some to a lesser degree than that seen in sample J372-1.5.

Sample Z071-7.3(Z058) was loaded with 31 gm, resulting in an applied stress of 16.3 MPa. The sample crept in a manner similar to that of sample J372-1.5, as can be seen in Figure 3. A second piece from this sample was loaded in the

same manner, but the load was removed during the "slow creep" region of the curve. On a third specimen from sample Z071-7.3, we removed the load in the "fast creep" portion of the curve. These two samples will be compared for dislocation density and configuration by optical microscopy and Transmission Electron Microscopy (TEM) to determine if the model of dislocation pile up at the twin planes and punching through to give a very rapid creep behavior is accurate.

Figure 4 shows the deflection vs. time curve obtained for sample N140-10.3(Z058). This sample was loaded with 49.2 gm, resulting in a stress of 35.4 MPa, approximately twice that of the previous samples. From the Figure, it can be seen that the sample crept very quickly to a deflection of approximately 2 mm and then stayed at that level, without displaying the stepped character of the previous samples.

Two specimens from sample R485-7.5(Z058) were loaded with the same weight to confirm the accuracy of comparing the behavior of two specimens from the same sample under different loading conditions. As can be seen in Figure 5, the effect of loading the two samples with 16.8 MPa resulted in curves of similar shape with regions of high creep rate at a deflection of 0.3 mm in both samples. One sample reached this deflection in less time than the other sample, sample #1 taking just over two minutes while sample #2 reached this point in just over one minute. Sample #2 from this ribbon also reaches a second higher creep rate after approximately two minutes. The beginning of this higher creep rate are seen in sample #1 from this ribbon for times greater than approximately five minutes. Study of these two curves leads us to believe that qualitative comparisons can be made between samples from the same ribbons under different bending loads, but quantitative comparisons will

be inaccurate.

Discussion

To distinguish between power law creep (strain rate proportional to σ^n) and linear creep (strain rate proportional to σ), we made the following calculations.

If power law creep is dominating, the initial stress distribution will appear as

but the final stress distribution will be

The final stress distribution can be modelled, to a good approximation as

Such a simple model predicts that if the material does not change during the test, the creep curve should look like

where $S_f = [1.5^n]^{-1} S_i$. In general, the creep exponent is about 2.5-3, so the final slope should be

$$S_f = 0.3 \text{ to } 0.36 \cdot S_i$$

The experimental data from Figure 2 show

$$S_i = 2 \text{ mm/min}$$

$$S_f = 0.1 \text{ mm/min}$$

which is less than the 0.6-0.72 mm/min predicted by the theory. This indicates that the material does change during the test, that is, the material hardens as dislocations become entangled and immobilized.

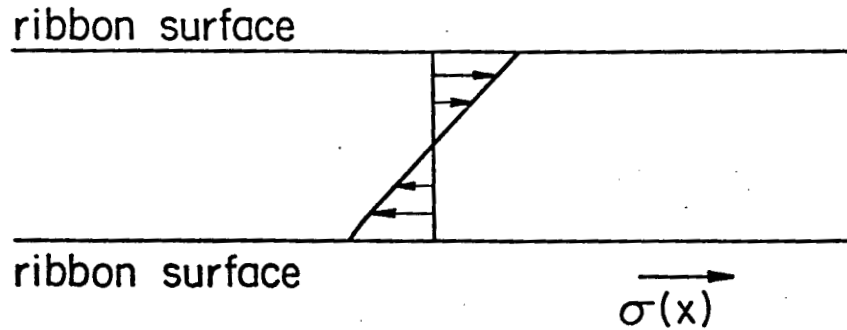
The initial slope of the deflection vs. time curve varies roughly like

be inaccurate.

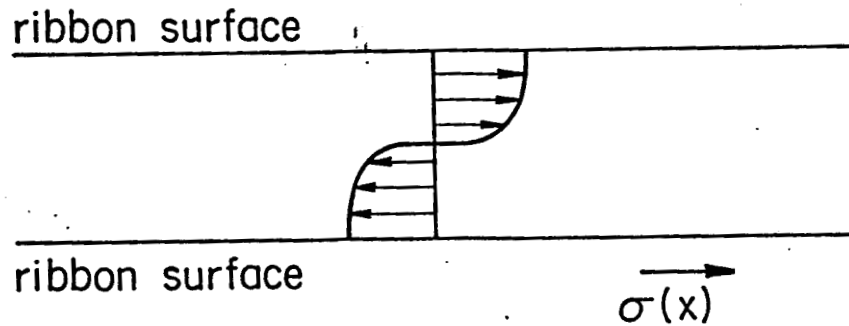
Discussion

To distinguish between power law creep (strain rate proportional to σ^n) and linear creep (strain rate proportional to σ), we made the following calculations.

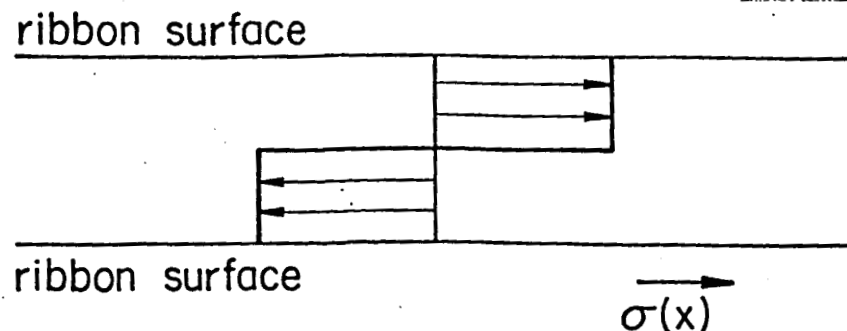
If power law creep is dominating, the initial stress distribution will appear as



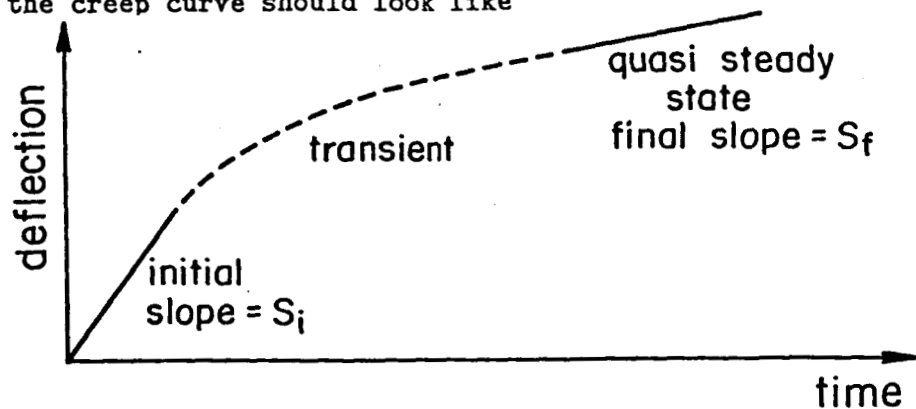
but the final stress distribution will be



The final stress distribution can be modelled, to a good approximation as



Such a simple model predicts that if the material does not change during the test, the creep curve should look like



where $S_f = [1.5^n]^{-1} S_i$. In general, the creep exponent is about 2.5-3, so the final slope should be

$$S_f = 0.3 \text{ to } 0.36 \cdot S_i$$

The experimental data from Figure 2 show

$$S_i = 2 \text{ mm/min}$$

$$S_f = 0.1 \text{ mm/min}$$

which is less than the 0.6-0.72 mm/min predicted by the theory. This indicates that the material does change during the test, that is, the material hardens as dislocations become entangled and immobilized.

The initial slope of the deflection vs. time curve varies roughly like

<u>Experiment</u>	<u>Applied Shear Stress</u>
2 mm/min	27 MPa
0.5 mm/min	16.3 MPa
6 mm/min	35.4 MPa
0.5 mm/min	16.8 MPa
0.5 mm/min	16.8 MPa

This follows a law of the form

$$S_i = \frac{\sigma^{2.5}}{1000} \dots \frac{\sigma^3}{7000}$$

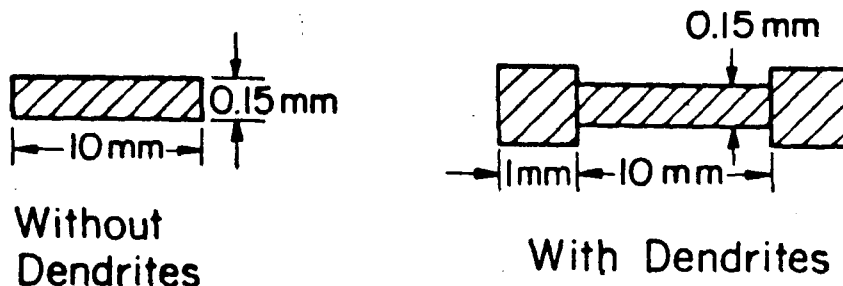
with σ in MPa and S_i in mm/min. This law then predicts

Experimental		Power Law Fit	
S_i (mm/min)	σ (MPa)	S_i (mm/min)	
		n=3	n=2.5
2	27	2.8	3.8
0.5	16.3	0.62	1.1
6	35.4	6.3	7.5
0.5	16.8	0.68	1.15
0.5	16.8	0.68	1.15

The fit to a power law type creep is not perfect, but the trend indicates that the creep we observe can be modelled in this way. As a final check, we can compare the data obtained from as sample with the dendrites on to those

obtained after removal of the dendrites to confirm that power law creep holds and we can model the behavior of the Web ribbons under an applied four-point bending using simple beam bending theory.

The initial slope of the curve obtained on the sample with the dendrites on was about 0.1 mm/min with an applied stress of 52.4 MPa. Modelling the ribbon/dendrite system as



it can be shown that the initial stress is almost totally carried by the dendrites. The maximum stress in the dendrite is, with the above geometry, only about one-quarter that in the non-dendrite part of the ribbon for the same loading. The effective stress in the dendrite is then about 13 MPa. From this stress, the strain rate is predicted to be approximately 0.3 mm/min using the power law derived above and $n=3$. Considering the experimental error and the very much simplified analysis, the predicted creep rate is in satisfactory agreement with the 0.1 mm/min observed for the sample. It therefore appears quite certain that the Web specimens creep according to a power law and that simple elastic or linear viscoelastic theory is inadequate. Our future measurements will employ numerical modeling.

Conclusions

Testing of the behavior of Web silicon under applied four point bending loads

was carried out at Mobil Solar Energy Corporation. Testing was done at 1000°C because the thin Web ribbons crept uncontrollably under the weight of the deflection probe at higher temperatures. The dendrites were seen to strengthen the ribbons considerably and testing was done on all subsequent samples after removal of the dendrites. The Web samples were seen to plastically deform as soon as the load was applied, as compared to Cz and FZ samples which have an "incubation time" for the formation of mobile dislocations. The Web ribbons also showed an unusual high creep-low creep behavior which we believe to be linked to the pile up and punch through of dislocations at the central twin boundaries.

Three samples from a single Web ribbon were bent under the same load but the test was stopped at various times to allow TEM investigation of the microstructure during the slow creep rate period and during the high creep rate period. Two samples from a different ribbon were tested under identical loads and lead us to believe that qualitative comparisons can be made between the samples from the same ribbon. One sample was subjected to a higher level of stress. It crept rapidly to a deflection of approximately 80 mils and then there was no further deformation.

These samples, as well as Cz and FZ samples subjected to four point bending, will be used for TEM studies of the microstructure of Web ribbons under stress.

Oxygen Measurements of Web Silicon

Experimental Design

A Nicolet 8000 model Fourier Transform Infra-red Spectrometer (FTIR) was used to measure the concentration of oxygen in Web Silicon. The beam size was approximately 4mm x 5mm. After the measurement the sample was removed from the beam and a background spectrum was taken. The spectrum obtained from the sample was divided by the background spectrum to remove any spurious absorption peaks due to the atmosphere or the detector. In ASTM calculation standard F 120-75, this method is called the Sample In-Sample Out method [12]. The Air Reference method, F 121-83, was used to calculate the concentrations of interstitial oxygen present in the samples. According to this reference the absorption coefficient, α , at the wavenumber of the absorption by interstitial silicon, 1106 cm^{-1} is multiplied by 4.9 to obtain the level of interstitial oxygen in ppma, and it is multiplied by 2.45×10^{17} to obtain the concentration of interstitial oxygen in atoms/cm³ at 300°K.

Since the Web ribbons are very thin, typically 100-150 microns, multiple reflections of the IR beam in the sample presented a great deal of difficulty. Multiple reflections cause a periodic variation in the transmitted intensity

vs. wavelength. All samples measured by infrared transmission show this effect of multiple internal reflections, but in thick samples the intensity varies so rapidly with wavelength that the variations are not resolved by the detection system. However, in thin samples, such as Web ribbons, the intensity variations from the multiple reflections are sufficiently gradual to be resolved by the detection system. Figure 7 shows the intensity variations caused by multiple reflections in the infrared transmission signal. To suppress these oscillations, we applied a 2.25 micron thick coating of ZnS to the ribbon surface to act as an anti-reflection coating [13], but the coating proved too uneven over the areas being measured to be of any benefit. In fact, the addition of the ZnS coating created more modes of internal reflection and made the measurement even more difficult. We believe that if a good ZnS coating was applied to the surface of a Web ribbon, oxygen measurements would be more reliable. We will continue work on developing a suitable coating method.

One benefit of using FTIR instead of standard single scan spectrometry is that the signal from the sample is collected and stored as an interferogram in Fourier Transform space, and can be edited to remove some of the effects of the multiple reflections. Specifically, the frequency corresponding to multiple internal reflections can be removed from the interferogram and hence edited out in the plot of transmission vs. wavenumber.

Initially, the samples were mounted at right angles to the incident infrared beam resulting in a great deal of multiple reflection. In Figure 7, multiple reflections cause the strong sine wave modulating the transmission signal. The multiple reflections were so strong that their removal reduced the remaining transmission data to the point where the resulting transmission

versus wavenumber plot could not be analyzed. However, tilting the samples a few degrees away from perpendicular incidence removed many of the multiple reflection peaks and the edited results could thus be analyzed with confidence. With the exception of the sample in Figure 7, all samples measured were held a few degrees off the vertical. The resulting interferogram was edited by deleting all contributions to the signal above 1300 cm^{-1} .

The thinness of the Web ribbons also complicates the infrared measurements because the strength of the transmitted signal is related to the volume sampled. That is, the strength of the absorption, and therefore the height of the absorption peak, is proportional to how many bonds of a particular type are encountered in the volume tested. Since the Web ribbons are thin, the volume sampled by the 4mm x 5mm beam is small, and many scans of the sample had to be superimposed to raise the signal above the level of the noise. In our measurements, the samples were each scanned 1000 times for a single set of data, whereas a typical infrared sample would require only about 32 scans for an acceptable signal level to be obtained. Measurement at low temperature would also enhance the signal and allow us to use fewer scans for a reliable signal, but this approach was not available on the system used and so is not included in this report.

Experimental Results

Figure 7 is the transmission spectrum of sample J 376-4.3 from 800 to 1300 wavenumbers(cm^{-1}). This region of the spectrum contains information about the interstitial oxygen as well as any information about SiO_x that is present, so

all spectra presented will be restricted to this range.

As can be seen from the Figure, a distinct sine wave is contained in the transmission signal. The envelope of this spectrum was entered into our computer and the arithmetic average signal was computed in an attempt to uncouple the sine wave from the information-containing transmission signal. The thickness of the Web sample was determined from the frequency of the sine wave to be about 150 microns in good agreement with the direct measurement.

Figure 8 was obtained after removing multiple reflections from Figure 7. Comparison of the Web spectrum in Figure 8 with the spectrum shown in Figure 9 obtained from a Czochralski (Cz) grown sample shows the following features. Firstly, the average transmission level of the Web ribbon is higher than that of the Cz sample, approximately 57% for the Web as compared to approximately 48% for the Cz in the flatter parts of the curves. Theory predicts a transmission of 51% for Si the thickness of the Cz sample, approximately 400 microns, and 53% for Si the thickness of the Web sample, approximately 150 microns. The Cz sample transmission is less than predicted, probably due to free carrier absorption not accounted for in the theory. However, the Web sample transmits more than theory predicts. This increase in transmission could be due to an oxide on the ribbon surface acting as an anti-reflective coating, or perhaps due to the sample shape acting to reduce reflection over the value predicted by a theory based on two parallel surfaces. It is not likely that there is a surface oxide on these samples thick enough to act as an anti-reflective coating, so we will study the effect of sample shape on the IR transmission in future experiments. Even though the Web sample is much thinner than the Cz sample, the height of the peak associated with interstitial oxygen at 1106 cm^{-1} is seen to be larger for the Web ribbon than

for the Cz sample, a height of 3.6% for the Web and 2.7% for the Cz. This larger peak indicates a much higher oxygen content for the Web ribbon. Calculations show an oxygen level of 25.3 ppma ($1.3 \times 10^{18} \text{ cm}^{-3}$) for the Web and 3.8 ppma ($1.9 \times 10^{17} \text{ cm}^{-3}$) for the Cz sample. Since the maximum solubility of oxygen in silicon at the melting temperature of silicon is about $3 \times 10^{18} \text{ cm}^{-3}$ the Web material is nearly saturated with oxygen at the growth temperature.

The most striking difference between the spectrum for the Web ribbon and the spectrum for the Cz sample is, however, the noticeable shoulder at about 1060 cm^{-1} on the interstitial oxygen peak in the Web ribbon. This shoulder has been attributed in the literature to a high pressure phase of SiO_2 called coesite, which forms in single crystal non-dislocated silicon on heat treatment at approximately 600°C . This phase is found to be unstable at higher temperatures except when dislocations are present, in which case the coesite is assumed to remain stable in the dislocation core. Figure 10 is taken from Koguchi, et al. [5], and shows the distinct shoulder on the interstitial oxygen peak formed both by annealing non-dislocated silicon at 600°C and by deforming silicon to create dislocations at high temperature. It can also be seen that the shoulder disappears from the non-dislocated sample at heat treatments at 900°C as the peak associated with the more stable phase of amorphous SiO_2 at 1225 cm^{-1} appears. In the dislocated crystal, however, the shoulder associated with coesite continues to grow with heat treatments at 900°C . Because the Web ribbons contain a great many dislocations, some intersecting the surface and some pinned at the central twin planes, it is likely that the behavior of oxygen in Web ribbons follows that of the dislocated sample investigated by Koguchi et al.

These two peaks can be separated as shown in Figure 11 for the sample in

Figure 8 into two distinct peaks, one associated only with the interstitial oxygen at 1106 cm^{-1} , and the other reflecting only the absorption by the coesite phase centered at approximately 1060 cm^{-1} . It can be seen in the Figure that the peak associated with the interstitial oxygen in the spectrum taken on the Web sample is broader than on the spectrum taken on the Cz material, shown in Figure 9. The Full Width at Half Maximum (FWHM) is 48.5 cm^{-1} for the Web interstitial oxygen peak and about 33 cm^{-1} for the Cz interstitial oxygen peak. The broadening of the interstitial oxygen peak is assumed to be related to stress in the silicon, but no quantitative data relating sample stress to peak width has been located. Although the internal stress of this Web ribbon is not known, the broad interstitial oxygen peak indicates that the internal stress is greater in the Web ribbon than in the Cz sample. We will investigate further whether the level of stress in the Web ribbons correlates with the width of the interstitial oxygen peak. Since the ASTM standard requires that the FWHM be less than 32 cm^{-1} for accuracy in the use of the standard, the Web Silicon peaks cannot be strictly interpreted by the ASTM standard. Another method, such as Secondary Ion Mass Spectrometry (SIMS), will have to be used to determine the accuracy of the ASTM standard calculations for use in measuring the oxygen content of Web silicon. Since SIMS and other atomic counting methods of measuring oxygen in silicon measure the total number of oxygen atoms and give no information about the binding states of the oxygen in the silicon, direct comparison of the size of the interstitial oxygen peak measured by IR absorption to the number of oxygen atoms counted by another method will not be straightforward. We are considering the possibility of relating the area under the IR absorption curve to the total number of oxygen atoms for direct comparison with other methods such as SIMS. The peak associated with the coesite phase of SiO_2 is also wide, for sample J 376-4.3 the FWHM is 57.6 cm^{-1} with a peak height of 2.2%.

The amount of oxygen present as coesite cannot be calculated in a straightforward manner, since there is no ASTM standard for the measurement of coesite in silicon.

Figures 12, 13 and 14 show the spectra for Web ribbons grown in various growth configurations. Figure 12 depicts the spectra of two different samples grown in the low stress Z058 configuration. As can be seen, sample N128-19.1 shows the distinct shoulder seen in the previous sample. However, another Z058 sample, N140-10.3, did not exhibit any shoulder at all. The interstitial oxygen content of these two ribbons is 19.8 ppma ($9.9 \times 10^{17} \text{ cm}^{-3}$) for sample N128-19.1, and 18.6 ppma ($9.3 \times 10^{17} \text{ cm}^{-3}$) for sample N140-10.3. The FWHM for sample N128-19.1 is 43.3 cm^{-1} . Figure 13 shows the spectra obtained from two samples grown in the relatively high stress configuration J435. Again, the shoulder can be seen distinctly on one sample, 2284-15.8, and is nearly absent in the other sample, 2-305-5.11. The interstitial oxygen content calculated for these samples was 17.3 ppma ($8.7 \times 10^{17} \text{ cm}^{-3}$) for sample 2284-15.8, and 18 ppma ($9 \times 10^{17} \text{ cm}^{-3}$) for sample 2-305-5.11. Their FWHM are 43.3 cm^{-1} for sample 2284-15.8, and 37 cm^{-1} for sample 2-305-5.11. Two samples from the third growth configuration for which samples were available, J460, did not show any development of a shoulder on the interstitial oxygen peak as can be seen in Figure 14 for sample R479-13.2. This sample was measured to have an interstitial oxygen content of 20 ppma ($1 \times 10^{18} \text{ cm}^{-3}$), and a FWHM of 36 cm^{-1} . Another measurement taken approximately 10 cm away from the area described by the spectrum in Figure 14 showed the same oxygen content, but had a FWHM of 39.7 cm^{-1} . The appearance of the shoulder associated with the presence of a coesite phase in the Web material does not seem to correlate with the growth configuration. Since only a small number of J460 samples were tested, the fact that the coesite shoulder did not appear in the spectra from these

samples can not be considered to prove that the coesite phase does not exist in the ribbons grown in the J460 growth configuration. The FWHM of the interstitial oxygen peak cannot be said to correlate with the growth configuration of the ribbon, but we need to study more samples to be sure of this.

Figure 15 shows the spectra for the same sample as shown in Figure 14, R479-13.2(J460), but now also includes the spectrum taken before a hydrofluoric acid etch was used to remove the dark blue surface oxide or oxy-nitride resulting from the growth ambient. This oxide is approximately 1000 Å. It can be seen that this heavy surface oxide creates a shoulder on the interstitial oxygen peak indistinguishable from that of the coesite phase. The surface oxide signal also interferes with accurate measurement of the interstitial oxygen content, which was calculated as 32.7 ppma ($1.6 \times 10^{18} \text{ cm}^{-3}$) with the oxide on the surface and 20.3 ppma ($1 \times 10^{18} \text{ cm}^{-3}$) after removal of the oxide layer. This demonstrates that in these samples the surface oxide needs to be thoroughly removed before any IR measurements are performed to determine the oxygen content and oxygen binding. All samples were HF etched before IR measurements to preclude the confusion over interpretation of the IR transmission vs. wavenumber data.

A scan along the length of sample N128-19.1(Z058) showed little change in the oxygen content or oxygen binding state along the growth direction. Figure 16 shows two spectra taken on this sample approximately 20 cm apart. The interstitial oxygen content changes by about $1.1 \times 10^{17} \text{ cm}^{-3}$, or 2.4 ppma, but the coesite shoulder appears more distinct in the sample with the lower interstitial oxygen content. We speculate that there is an approximately constant amount of oxygen in the Web ribbons, close to the maximum solubility

of oxygen in silicon, and that the oxygen is present either as interstitial oxygen or as oxygen in the SiO_2 coesite phase, perhaps associated with dislocations in the material.

A scan was also made across the width of sample Z025-3.7A(J435), and three of the spectra are shown in Figure 17. The resolution obtained with a 4 mm beam scanning across a 2 cm ribbon is low, but some trends can be discerned from the data. Figures 0-10a and 0-10c are near the two dendrites at the edge of the sample and Figure 0-10b was taken near the center of the sample. The interstitial oxygen content appears to decrease slightly in the center of the ribbon compared to the edges near the dendrites. For this Figure, the interstitial oxygen content near one dendrite is calculated to be 19 ppma ($9.5 \times 10^{17} \text{ cm}^{-3}$), 18 ppma ($9 \times 10^{17} \text{ cm}^{-3}$) near the ribbon center, and 22 ppma ($1.1 \times 10^{18} \text{ cm}^{-3}$) near the other dendrite. It is not clear whether this is a significant change in the measured interstitial oxygen content and more scans will be carried out to confirm or reject this trend. We will also attempt to improve the resolution of this measurement, but using a smaller beam will decrease the signal, making the detection of the oxygen peak more difficult.

Finally, oxygen measurements were performed on samples with a known amount of internal stress. These samples were obtained from Westinghouse where adjacent pieces of material had been etched to determine the amount of residual stress in the ribbon. Figure 18 shows the spectra from samples Z025-3.7A(J435) and R461-5.7-A(J460L). The interstitial oxygen content appears slightly lower in sample Z025-3.7A, 18.8 ppma ($9.4 \times 10^{17} \text{ cm}^{-3}$), versus 20.5 ppma ($1 \times 10^{18} \text{ cm}^{-3}$) for sample R461-5.7-A. Sample Z025-3.7A is also the sample with the higher residual stress, measured as 40 Mdyn/cm as opposed to -3 Mdyn/cm for sample R461-5.7-A by the etch-pit counting technique developed by Westinghouse. The

shapes of the two spectra are also similar, indicating that there is no significant difference in the configuration of the oxygen, that is, the ribbons with the higher residual stress do not seem to contain the coesite phase at higher concentrations than ribbons with a low residual stress. The FWHM for the two samples are; 43.3 cm^{-1} for the high stress sample, Z025-3.7A, and 35.4 cm^{-1} for the sample with the lower residual stress, R461-5.7-A. This agrees with the supposition that the width of the interstitial oxygen peak increases with residual stress in the sample. It is not known whether the difference in interstitial oxygen content between these two ribbons is significant or if it is related to the residual stress in the ribbons. Further work will be carried to determine if there is any correlation between the oxygen content and configuration, and the stress in the ribbon.

Conclusions on Oxygen Measurements

The interstitial oxygen content of the Web samples measured by FTIR is consistently high, ranging between 18 and 22.5 ppma ($9 \times 10^{17} \text{ cm}^{-3}$ and $1.1 \times 10^{18} \text{ cm}^{-3}$), where the maximum solubility of oxygen in silicon near the melting point of silicon is about $3 \times 10^{18} \text{ cm}^{-3}$. Some Web samples display a shoulder on the interstitial oxygen absorption peak which coincides with the IR absorption of coesite, a high pressure phase of SiO_2 . According to the literature, this phase is present in non-dislocated single crystal silicon after heat treatments in the vicinity of 600°C , as well as in single crystal silicon with dislocations. The coesite phase is not stable in non-dislocated single crystal silicon at temperatures above approximately 800°C . Further tests including etching and optical microscopy, TEM and FTIR will be carried

out on the Web ribbons to determine if the coesite in the Web ribbons is present as free precipitates that dissolve at high temperatures or if it is associated with dislocations, in which case the coesite will be stable up to temperatures at which the oxygen can redissolve into the silicon matrix, about 1200°C [5].

The interstitial oxygen content and the appearance of the coesite shoulder do not seem to correlate with the growth configurations studied, J435, J460 and Z058. Furthermore, some samples grown in either the J435 or the Z058 configuration lacked the shoulder associated with coesite, while other samples from the same growth configuration did display this shoulder. Neither of the J460 samples tested showed the coesite shoulder, but we do not feel that this small sampling indicates that the coesite phase does not form during the ribbon growth in the J460 configuration.

The peaks associated with interstitial oxygen were seen to be wider for the Web samples than for the Cz sample. In fact, these peaks are wider than the ASTM allows for proper use of the calculation from absorption coefficient to the interstitial oxygen content. The peak broadening is thought to be related to the internal stresses in the Web ribbons, but no trends with growth configuration have been discerned.

The surface oxide present on some samples as a result of temperature and ambient seen by the ribbons during growth was found to interfere with both the identification of the coesite shoulder and the quantitative measurement of the interstitial oxygen content. It was concluded that samples must be etched in HF prior to FTIR to measure oxygen reliably.

The oxygen content was not seen to change significantly along the growth direction in the sample measured. There seemed to be some indication that the interstitial oxygen content to be higher near the dendrites than in the ribbon center in the one sample tested, but the change was so slight that more data are needed to confirm this behavior and determine if the change is significant.

For the two samples obtained from Westinghouse with a known amount of residual stress there seemed to be no correlation between the amount of stress in the ribbon and the interstitial oxygen content or the presence of the coesite SiO_2 phase. The peak width for the sample with a higher amount of residual stress was greater than that for the sample with a lower amount of residual stress, correlating with the theory that the peak width is increased with increasing sample stress.

Further measurements will be carried out to determine any correlation between the amount and state of oxygen in the Web ribbons and the stress in the ribbon, the growth configuration of the ribbon and the position within the ribbon, i.e., in the center of the ribbon as opposed to near the dendrites.

Although the use of a ZnS anti-reflective coating on the surface of the Web ribbons was not successful on the first attempt, we believe that the use of an anti-reflective coating may make data manipulation in the Fourier Transform space unnecessary, and make the curves of transmission vs. wavenumber more reliable. We will continue work on this aspect of the oxygen measurements.

Surface Profiles of Web Ribbons

Lateral profiles of the surfaces of Web ribbons were determined using a Tallysurf 5-120 Surface Profilometer. The profiles were taken to check the accuracy of using the thickness of the Web ribbons calculated from the Fourier Transform Infrared (FTIR) interferograms in the calculations of the interstitial oxygen content of the ribbons [14].

The transmission of the IR beam depends on the thickness of the silicon by

$$\frac{I}{I_0} = \exp\left(\frac{-x}{L}\right) (1-R)^2 (1-R^2 \exp(-2x/L))^{-1}$$

where

$$R = \left(\frac{n_1 - n_2}{n_1 + n_2}\right)^2$$

and

$$n_1 = 1.003 \quad (\text{air})$$

$$n_2 = 3.4181 \quad (\text{silicon at 9 microns}),$$

I_0 is the incident beam intensity, x is the distance in the silicon, and L is a characteristic absorption length, or optical depth, for light in the silicon. The value of L is dependent on the wavelength of the incident light. For wavelengths near that of the interstitial oxygen absorption peak, 9 microns, L is approximately 1 cm^{-1} , but the exact value depends on how the silicon was grown. Strictly speaking, the average thickness of the sample in the beam cannot be used since the thicker parts of the sample will dominate the absorption. However, when $x \ll L$, as in the case of Web ribbons, then the exponential term can be expanded as

$$\exp\left(\frac{-x}{L}\right) = 1 - \frac{x}{L} + \frac{x^2}{2L^2} - \dots$$

which, at about 9 microns, yields for oxygen free silicon

$$\frac{I}{I_0} = 0.5406 (1 - 1.46x + \dots) \quad (x \text{ in cm})$$

and the higher order terms can be neglected. Then, the thickness of the sample determines the absorption of the IR linearly. In Web ribbons, x is approximately 150 microns, much less than L and the absorption can be considered a linear function of the sample thickness.

Figure 18 shows the lateral surface profile of Web ribbon J376-4.3. The surfaces of the ribbon are smooth, but there is a large variation in the thickness across the ribbon from dendrite to dendrite. In this case, the center of the ribbon is approximately 30 microns thicker than the edges of the ribbon. The Web ribbon was measured to be 130 microns thick in the approximate ribbon center. The thinnest part of the ribbon is about 1 mm in

from the edge of the dendrite. This change in thickness of the ribbon over the area of the infrared beam in the FTIR makes determination of the interstitial oxygen content using an average thickness of the ribbon less accurate. The fact that the ribbon is significantly thinner at the edges will also complicate the measurement of oxygen content from dendrite to dendrite, making it difficult to determine if the oxygen content changes across the ribbon width or if the variation in ribbon thickness causes some error in the calculations.

Figure 19 shows a front surface lateral profile of the same sample as that in Figure 18, J376-4.3, but offset approximately 10 cm from the previous profile. On one side, the surface is similar to that shown previously, that is, narrow near the dendrite and increasing smoothly in thickness toward the ribbon center. On the other side, however, the ribbon does not get thinner toward the dendrite, but stays about the same thickness except within 2 mm of the dendrite, where the ribbon narrows drastically to join the dendrite as before. This wide variation longitudinal in surface profile over 10 cm of growth suggests that it would be impractical to try to determine the exact surface profile of an area measured by FTIR since a small error in the location of the IR beam results in a large error in the surface profile.

Figure 20 is an example of one of the widest ribbon thickness variations seen in the surface profile measurements. Sample RE343-3.3 has a 120 micron "hump" on one side of the ribbon and then tapers smoothly down to the other side. This ribbon was measured to be 150 microns thick at the approximate ribbon center, so the variation in thickness across the ribbon is a significant fraction of the measured ribbon thickness. Figure 21 is of the same area of RE343-3.3 as in the previous Figure at a lower magnification. In this Figure,

the thin part of the ribbon and the profile of the dendrite are shown. The thinnest part of the ribbon is again about 1 mm in from the dendrite and the ribbon joins smoothly into the dendrite. The profile of the dendrite is also quite smooth on this scale, while visually the dendrite is very jagged in appearance.

Conclusions

Surface profiles of the Web ribbons revealed that the ribbons are generally thicker in the center than at the edges, although this was not always seen to be the case. The lateral surface profile changes rapidly as the ribbon grows and can develop thickness variations from dendrite to dendrite on the order of the measured central ribbon thickness. This thickness variation will affect the accuracy of the calculations to determine the interstitial oxygen content, but since the surface profile changes rapidly we feel that using the average thickness over the IR measurement area as measured from the FTIR interferogram will provide the highest accuracy for the oxygen calculations.

Conclusions

The study of Dendritic Web silicon ribbons under applied stresses was begun during the reporting period September, 1984 to August, 1985.

The Web ribbons were found to behave unusually under four-point bending at 1000°C. The ribbons exhibited a fast creep-slow-creep behavior where slow creep began immediately on loading, followed by a short period of rapid creep. In some ribbons this pattern was seen to repeat more than once during the test. One ribbon tested under a larger stress did not exhibit this fast creep-slow creep behavior, but crept rapidly to a deflection of approximately 2 mm and remained at that level for the duration of the test. Our current model for this unusual creep behavior is one of initial easy movement of dislocations on loading until the dislocations encounter the obstacle of the central twin planes. The dislocations pile up at the twin planes until the stresses generated on the leading dislocation is great enough to cause the dislocations closest to the twin planes to punch through and travel to the other side of the ribbons, resulting in a short period of fast creep. Specimens prepared for investigation by Transmission Electron Microscopy will be studied in the next reporting period.

Measurements of the oxygen content of the Web ribbons also revealed unusual

behavior. The interstitial oxygen content was found to be consistently high, around 10^{18} cm^{-3} , near the solubility limit of oxygen in silicon at the melting point of silicon. The oxygen content seemed to change little along a 10 cm length of ribbon or across the width of one ribbon. The peak associated with interstitial oxygen in the Infrared Transmission spectrum was seen to be broad. This peak broadening has been associated with stress in silicon. In the two samples where the stress in the ribbon was known, the ribbon with the higher residual stress did have a broader interstitial oxygen absorption peak. The relationship between the measured stress in Web ribbons and the width of the interstitial oxygen peak will be studied in the upcoming year. In addition to the broad interstitial oxygen peak seen in the Web ribbons, a shoulder on this peak was seen in some ribbons. The appearance of the shoulder and its height could not be correlated with the ribbon growth configuration. This shoulder was not observed in the two ribbons from the J460 growth configuration studied, but we cannot assume that ribbons grown in this growth configuration do not ever exhibit this shoulder. The appearance of the shoulder did change slightly along a 10 cm length of ribbon. We currently believe that this shoulder is caused by the formation of SiO_2 coesite precipitates along the grown-in dislocations during the crystal growth. Further IR studies on samples that have been heat-treated and TEM investigation of the dislocations at the twin boundaries will be performed during the coming year to clarify the state of the oxygen in the Web ribbons.

Surface profiles of Web ribbons showed that the ribbons are generally thicker in the ribbon center by about 30 microns. The shape of the surface changes rapidly as the ribbon grows. We determined that the rapid changes in surface morphology would make any attempt to measure the exact area of a ribbon where oxygen measurements had been obtained to confirm the thickness of the ribbon

as measured by the IR beam fruitless. Therefore, we will continue to use the average thickness of the ribbon determined from the IR measurement for the calculation of the interstitial oxygen content.

References

1. O'Hara, S. and G. H. Schwuttke, J.Appl.Phys. 36 (1965), 2475.
2. Cunningham, B., H. Strunk and D. Ast, Defect Structure of Web Silicon, DOE/JPL Report 954852-5, October, 1980.
3. Gleichmann, R., M.D. Vaudin and D.G. Ast, "Recovery of Edge-Defined Film-Fed Grown Silicon", Phil.Mag.A 51(3) (1985), 449.
4. Doerschel, J. and F.G. Kirscht, "Differences in Plastic Deformation Behavior of Cz and FZ Silicon Crystals", Phys.Stat.Sol. A64 (1981), K85.
5. Koguchi, M., I. Yonenaga and K. Sumino, "Oxygen Donors Developed Around Dislocations in Silicon", Jap.J.Appl.Phys. 21 (1982), L411.
6. Ourmazd, A., W. Schroeter and A. Bourret, "Oxygen Related Thermal Donors in Si: A New Structural and Kinetic Model", J.Appl.Phys. 56 (1984),1670.
7. Pajot, B. and B Cales, "Infrared Spectroscopy of Interstitial O in Si", Materials Research Society Symposium Proceedings, Vol. 59, Oxygen, Carbon, Hydrogen and Nitrogen in Crystalline Silicon, Fall, 1985, to be published.
8. Kalejs, J.P., "Stress Studies in EFG", DOE/JPL Report 956312/83/04, April-June 1983.
9. Reed-Hill, R.E., Physical Metallurgy Principles, Second Edition, University Series in Basic Engineering, Litton Educational Publishing, Inc., Monterey, CA, 1973.
10. Beer, F.P., and E.R. Johnson, Jr., Vector Mechanics for Engineers:Statics, Second Edition, McGraw-Hill Book Company, New York, NY, 1972.
11. Ast, D.G. and D.J. Krenitsky, "Stress Relaxation in Coiled Ribbons of $Fe_{40}Ni_{40}P_{14}B_6$ and $Fe_{29}Ni_{49}P_{14}B_6S_2$ ", J.Mat.Sci. 14(1979), 287.
12. Annual Book of ASTM Standards, Volume 10.05.
13. Ohsawa, A, K. Honda, S. Ohkawa and R. Ueda, "Determination of O Concentration Profiles in Si Crystals Observed by Scanning IR Absorption Using Semiconductor Laser", Appl.Phys.Lett. 36(2),15 January,1980, 147.
14. Runyan, W.R., Silicon Semiconductor Technology, McGraw-Hill Book Co., New York, NY, 1965.

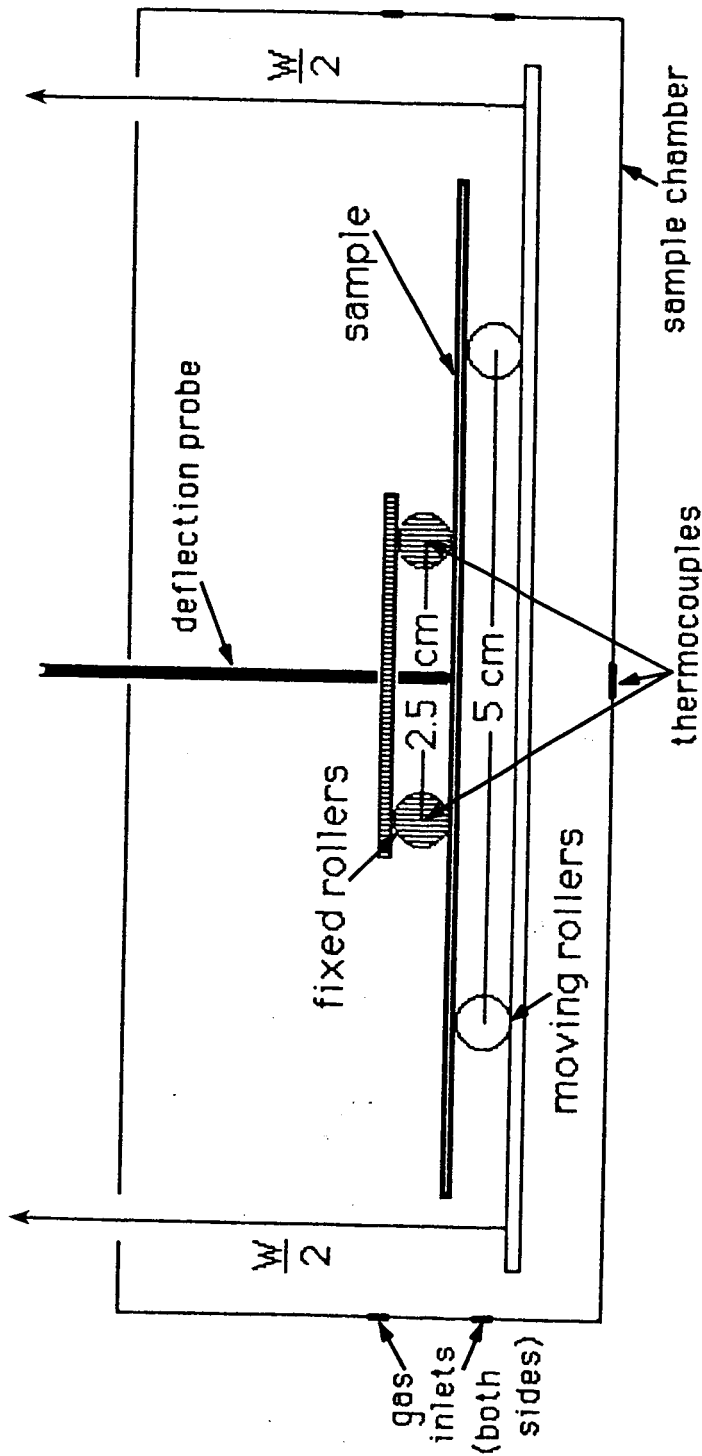


Figure 1: Schematic representation of the four point bending apparatus at Mobil Solar Energy Corporation, showing the distance between the fixed top rollers and the moveable bottom rollers. The applied weight, W , and the distance between the rollers determine the stress experienced by the sample.

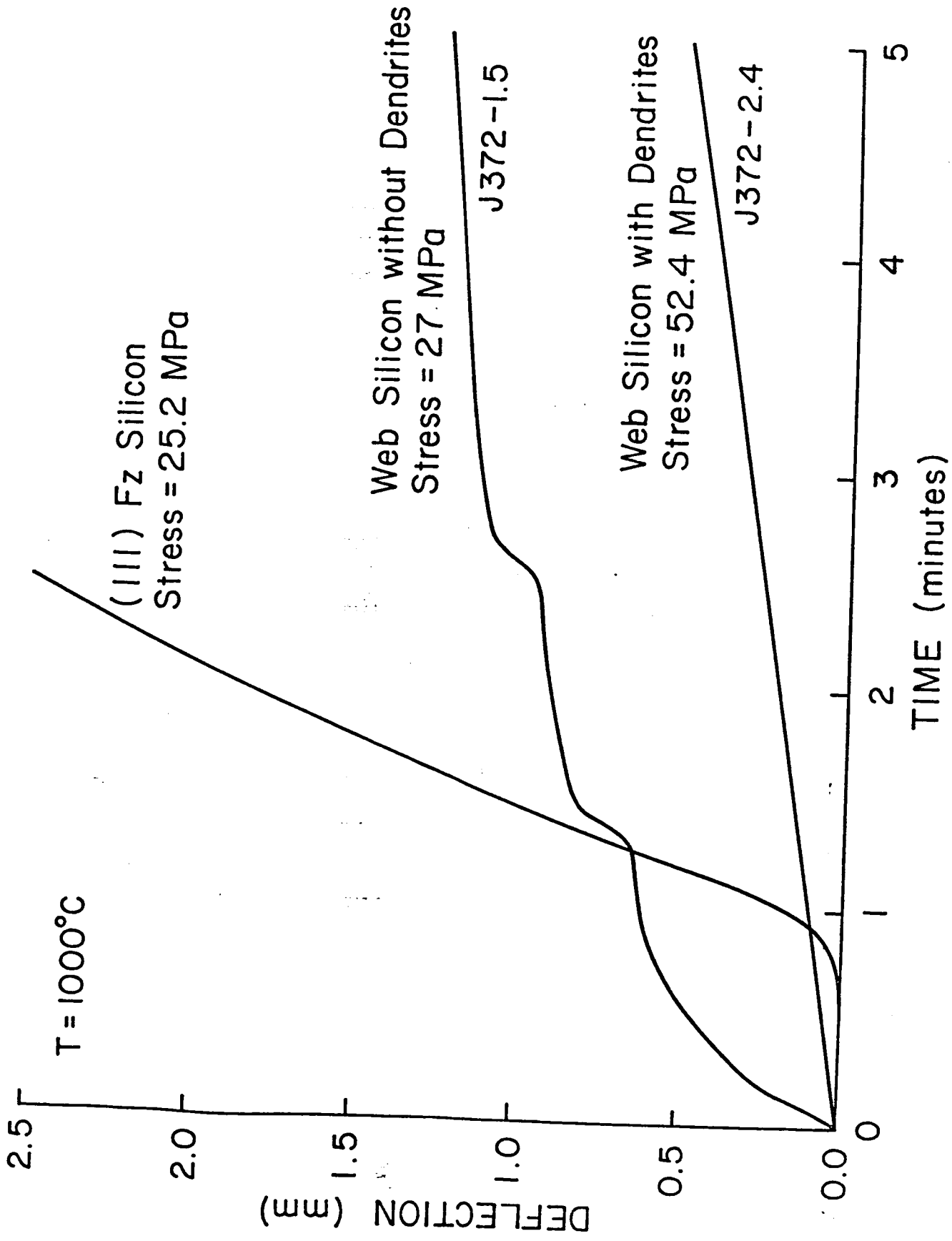


Figure 2: Deflection of the sample center vs. time for two Web samples and one Float Zone sample. The Web sample with the dendrites intact did not bend significantly under twice the stress encountered by the Web without dendrites and the FZ sample.

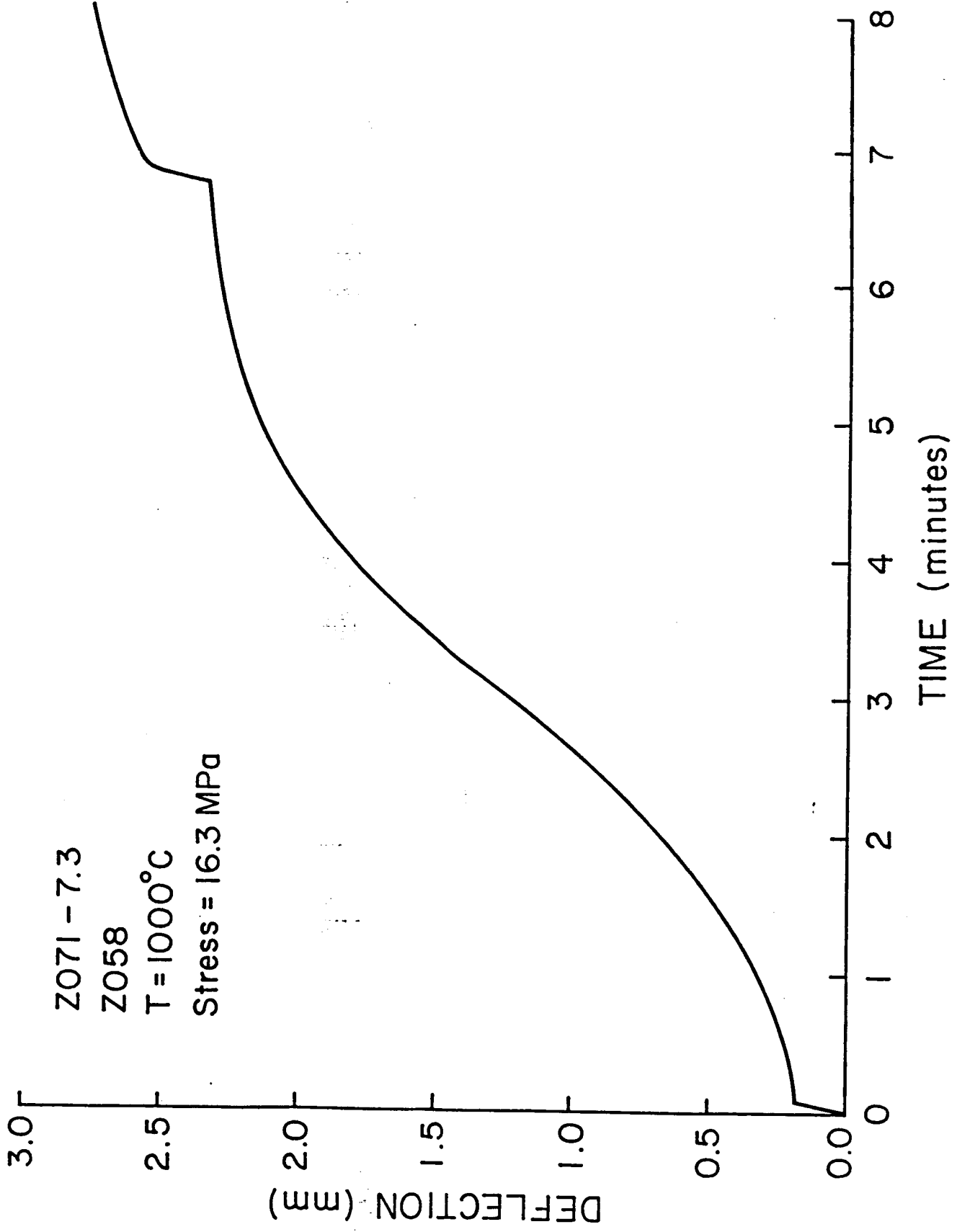


Figure 3: Deflection of sample center vs. time for Web sampl Z071-7.3.

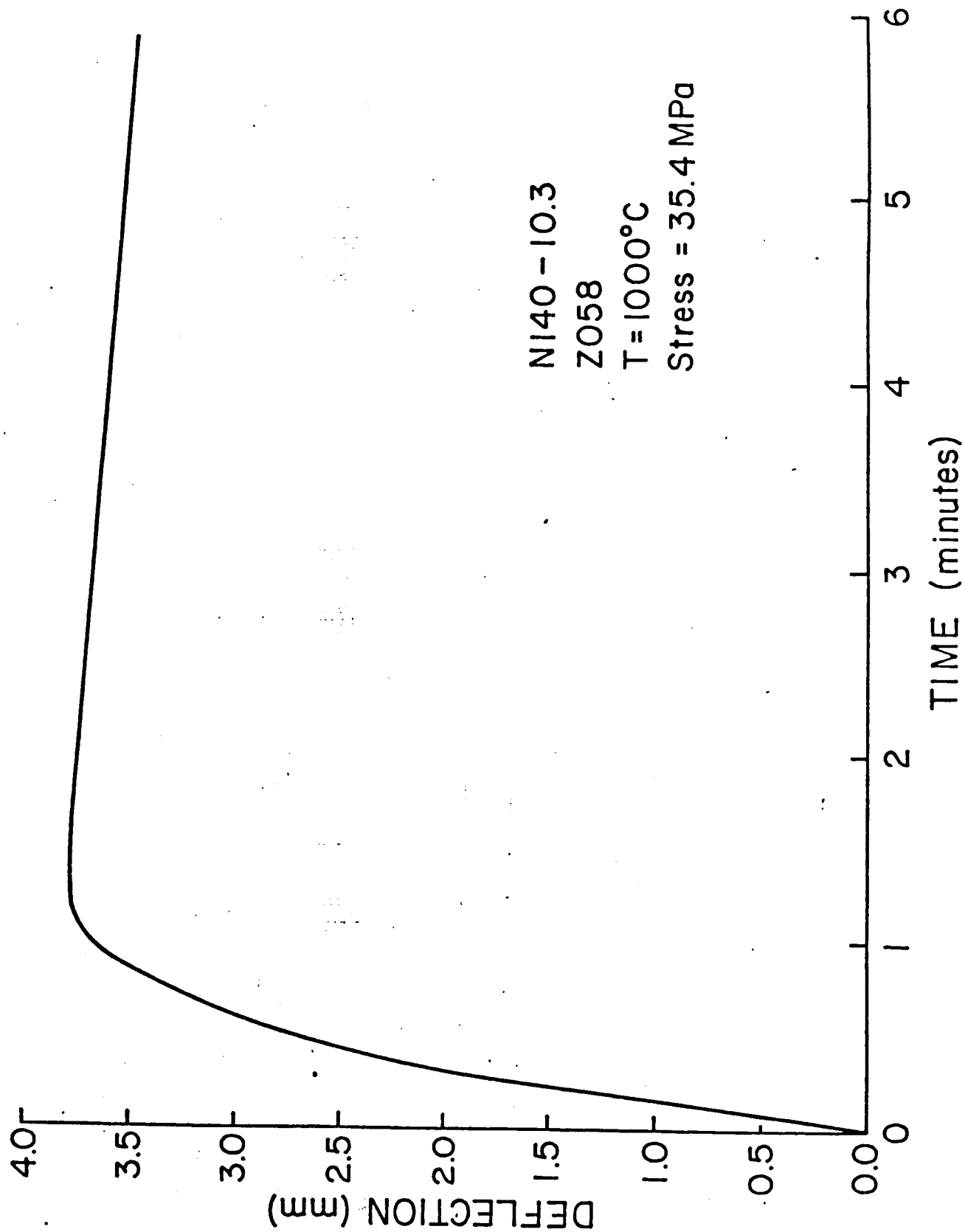


Figure 4: Deflection of sample center vs. time for Web sample NI40-10.3.

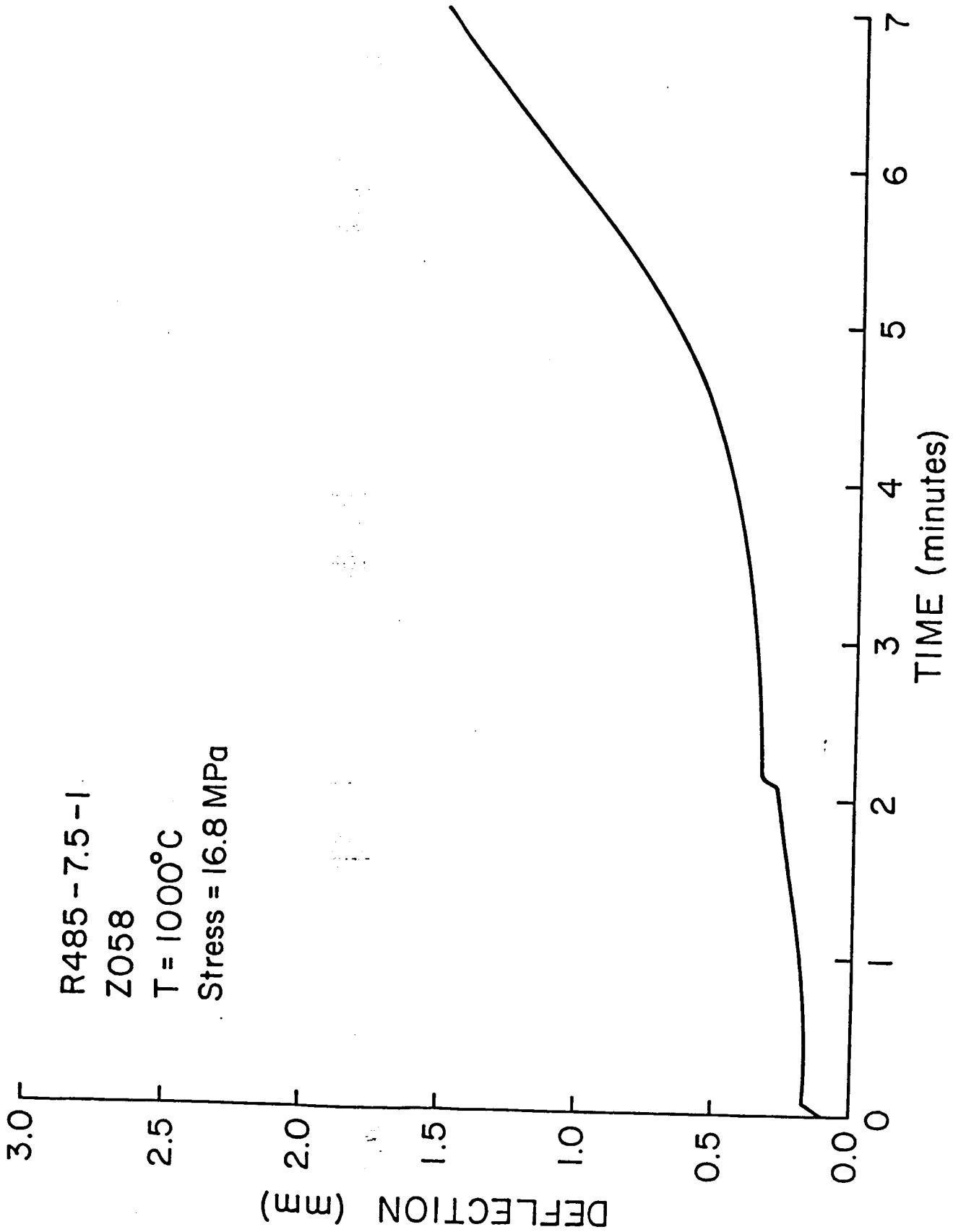


Figure 5: Deflection of sample center vs. time for Web sample R485-7.5-1. Compare this curve to the one shown in Figure 6 for another section of the sample ribbon under identical testing conditions.

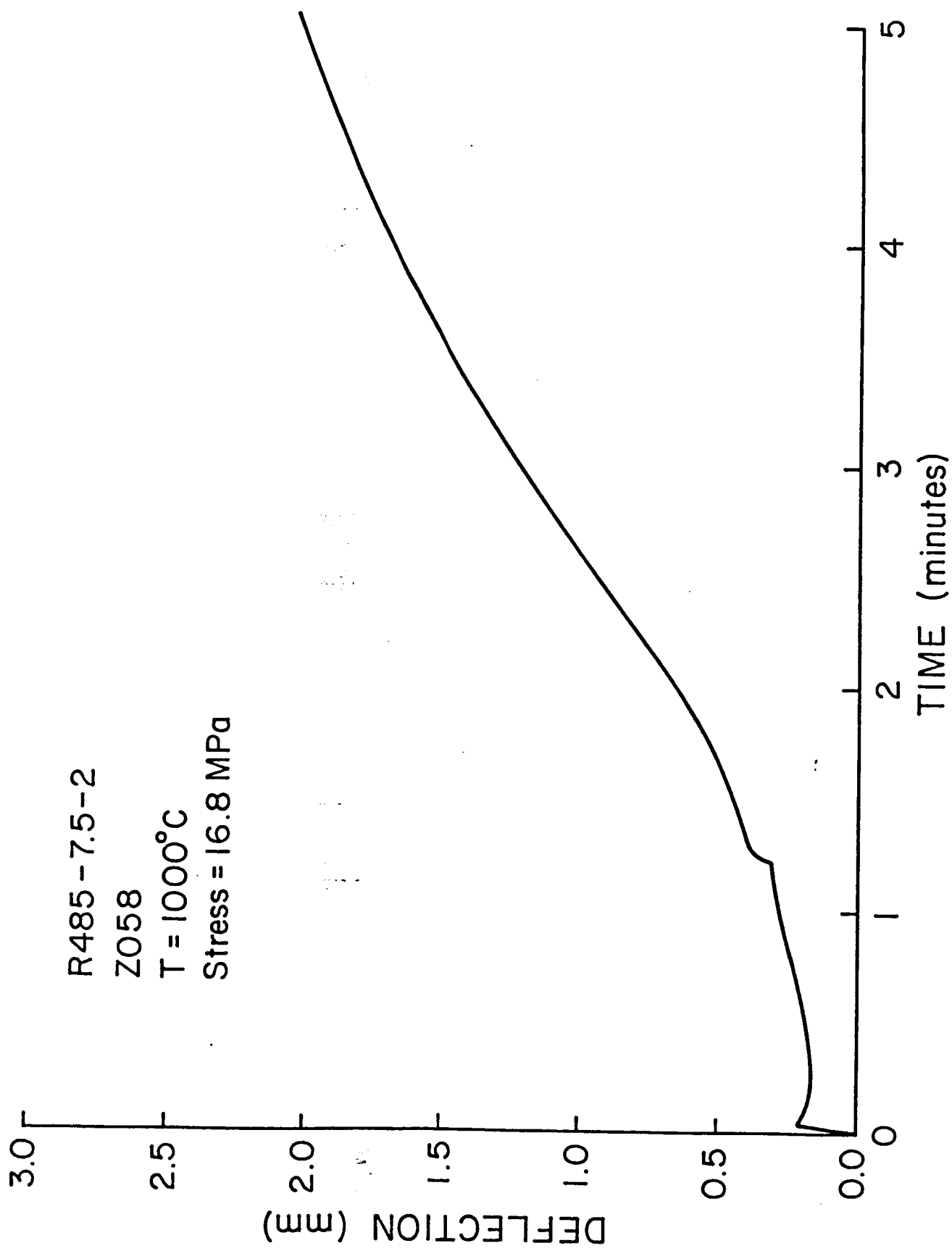


Figure 6: Deflection of sample center vs. time for Web sample R485-7.5-2. Compare this curve with the one shown in Figure 5 for another section of the same ribbon under identical testing conditions.

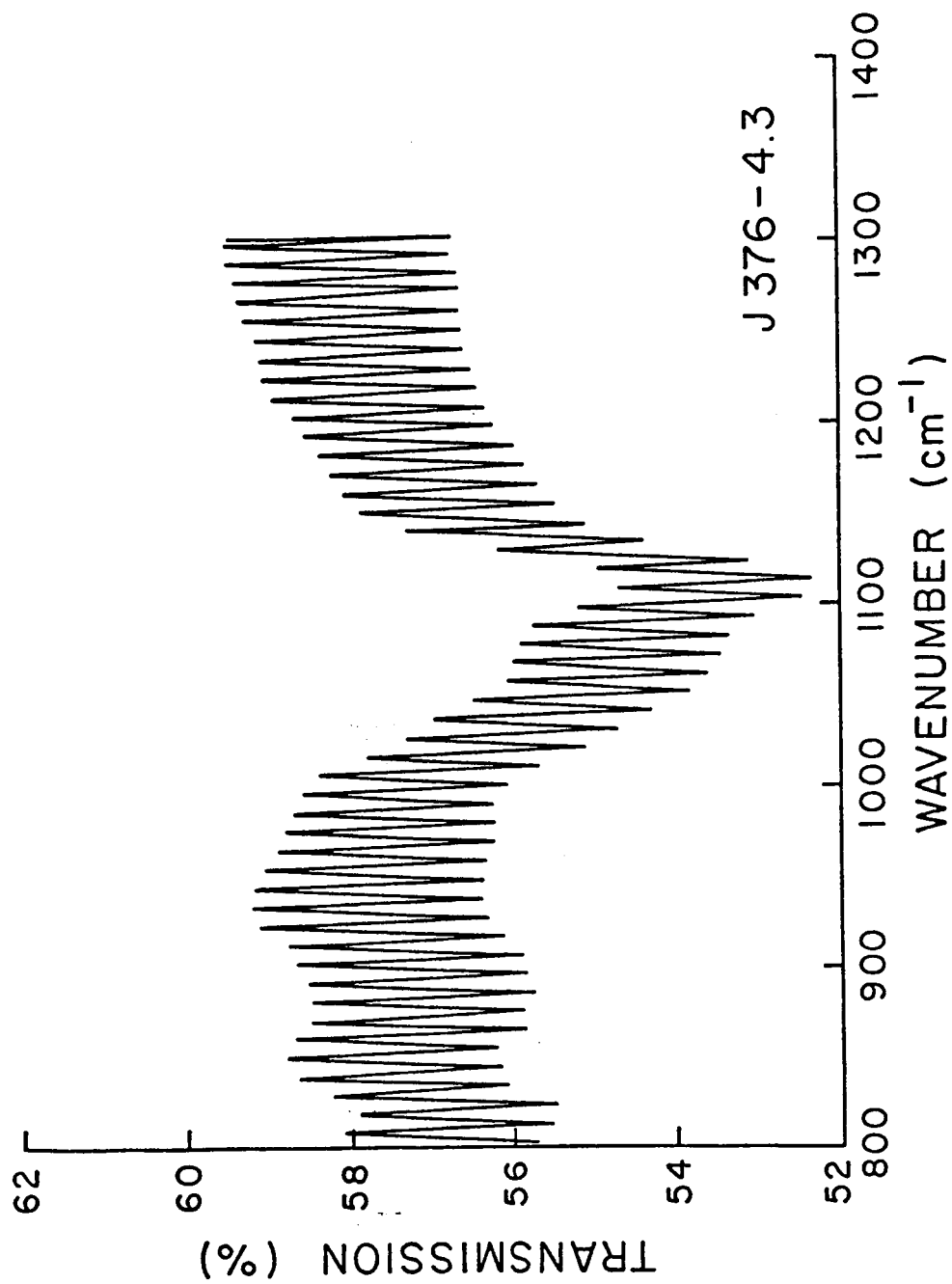


Figure 7: Intensity of the transmitted IR beam vs. wavenumber for Web sample J376-4.3 (1000 scans). The peak-to-peak distance corresponds to the thickness of the Web ribbon and is due to multiple internal reflections.

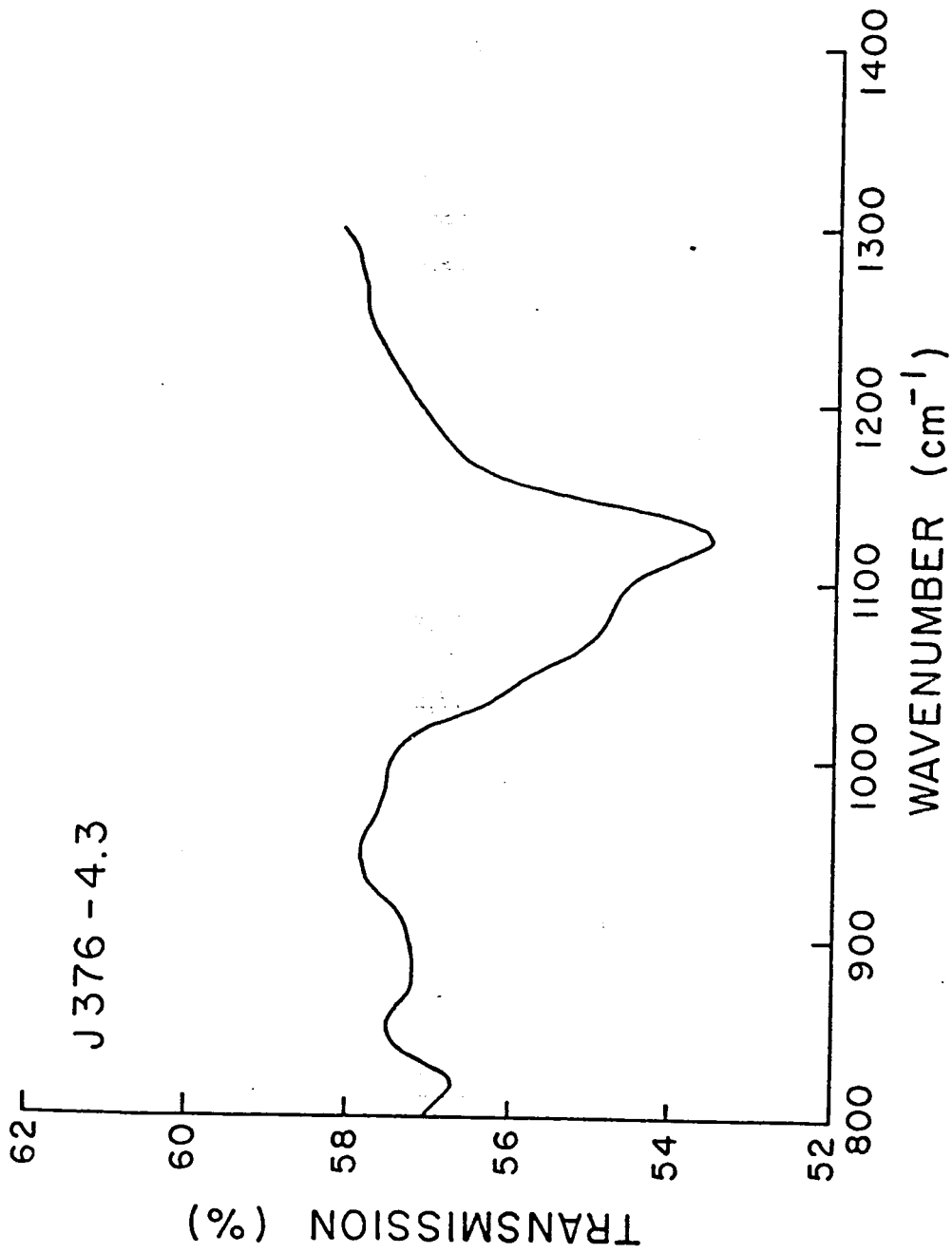


Figure 8: Intensity of the transmitted IR beam vs. wavenumber for the same sample shown in Figure 7, J376-4.3, after removal of the large sinusoidal variations seen in the previous Figure.

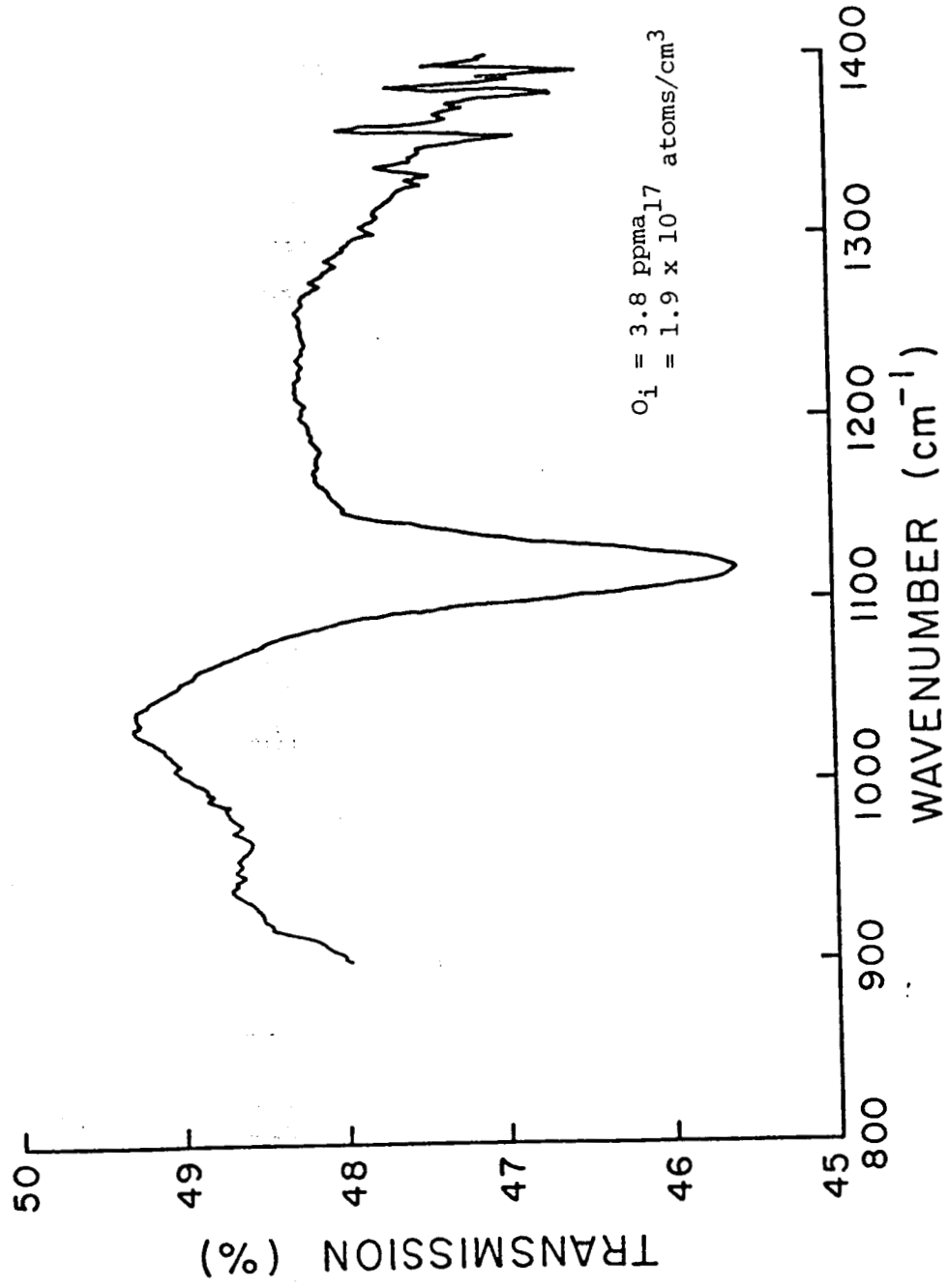
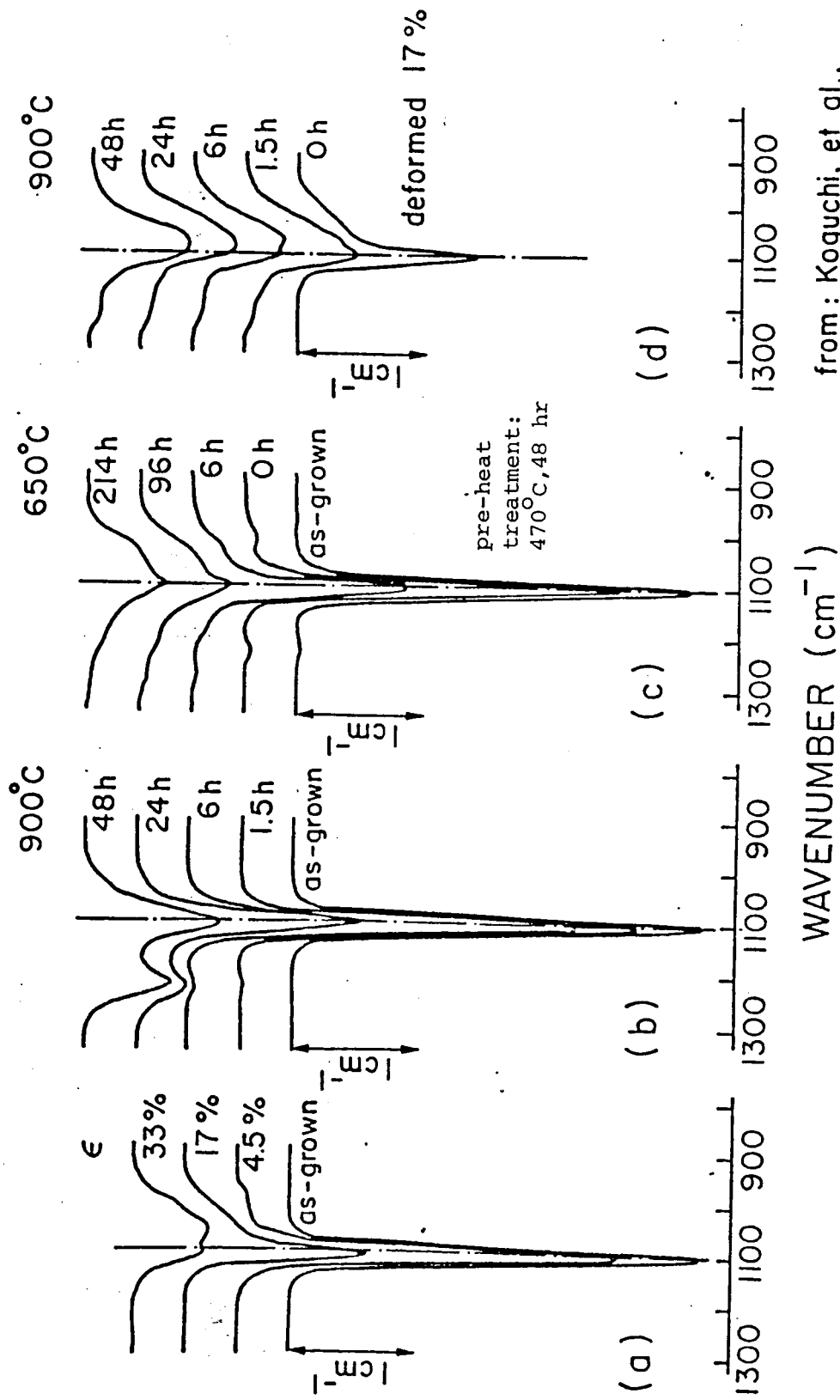


Figure 9: Intensity of the transmitted IR beam vs. time for a Czochralski sample.



from: Koguchi, et al.,
 Jap. J. Appl. Phys. 21, 7,
 pp. L411-L413.

Figure 10: Figure taken from Koguchi, et al., showing development of a distinct shoulder on the interstitial oxygen peak by heat treatment at 650°C for a non-defected crystal and by heat treatment at 900°C for a deformed crystal.

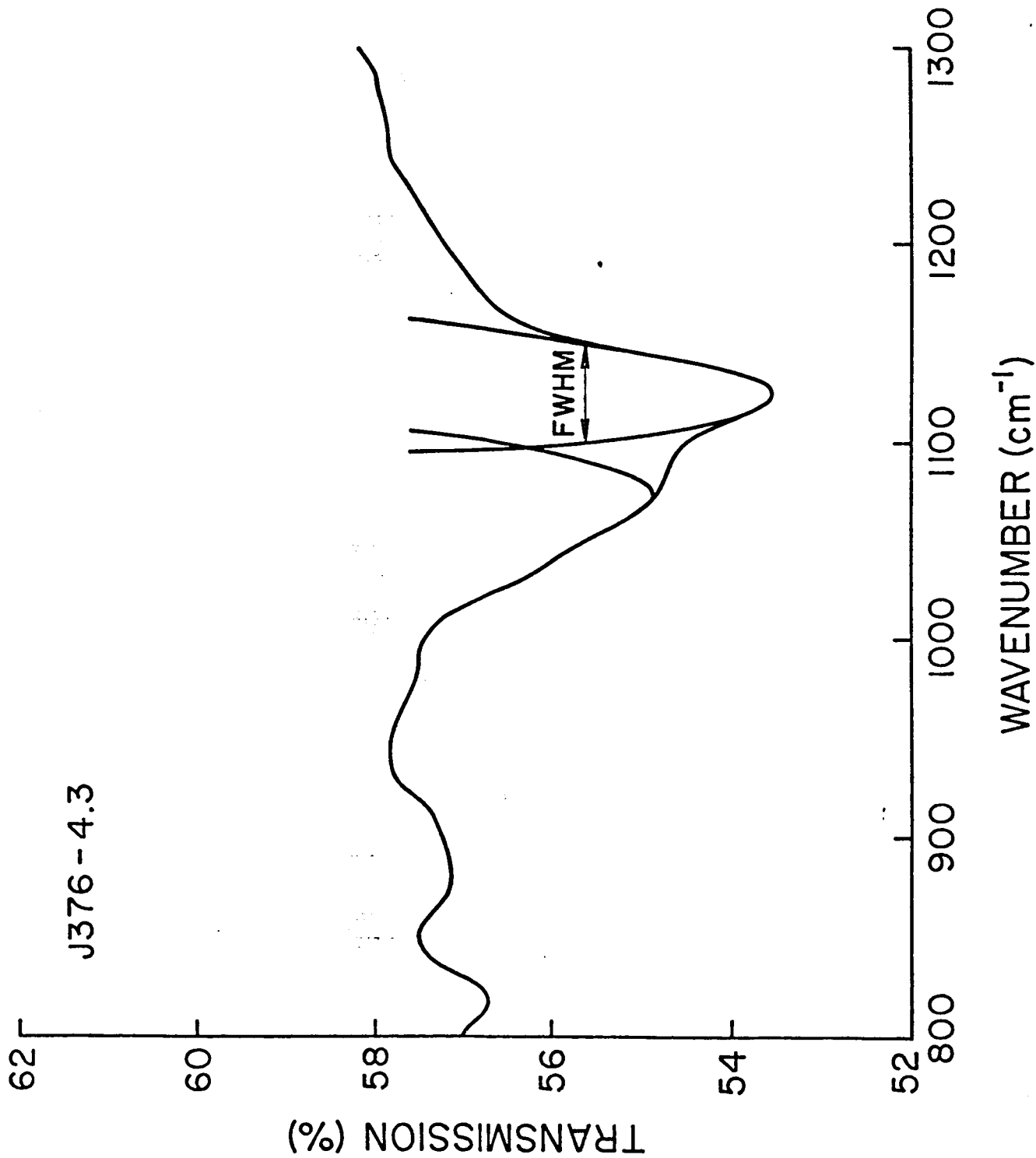


Figure 11: Data from Figure 8 deconvolved to reveal two peaks making up the single absorption peak plus a shoulder seen in some Web samples. FWHM is the Full Width at Half Maximum and is generally thought to be related to stress in the sample.

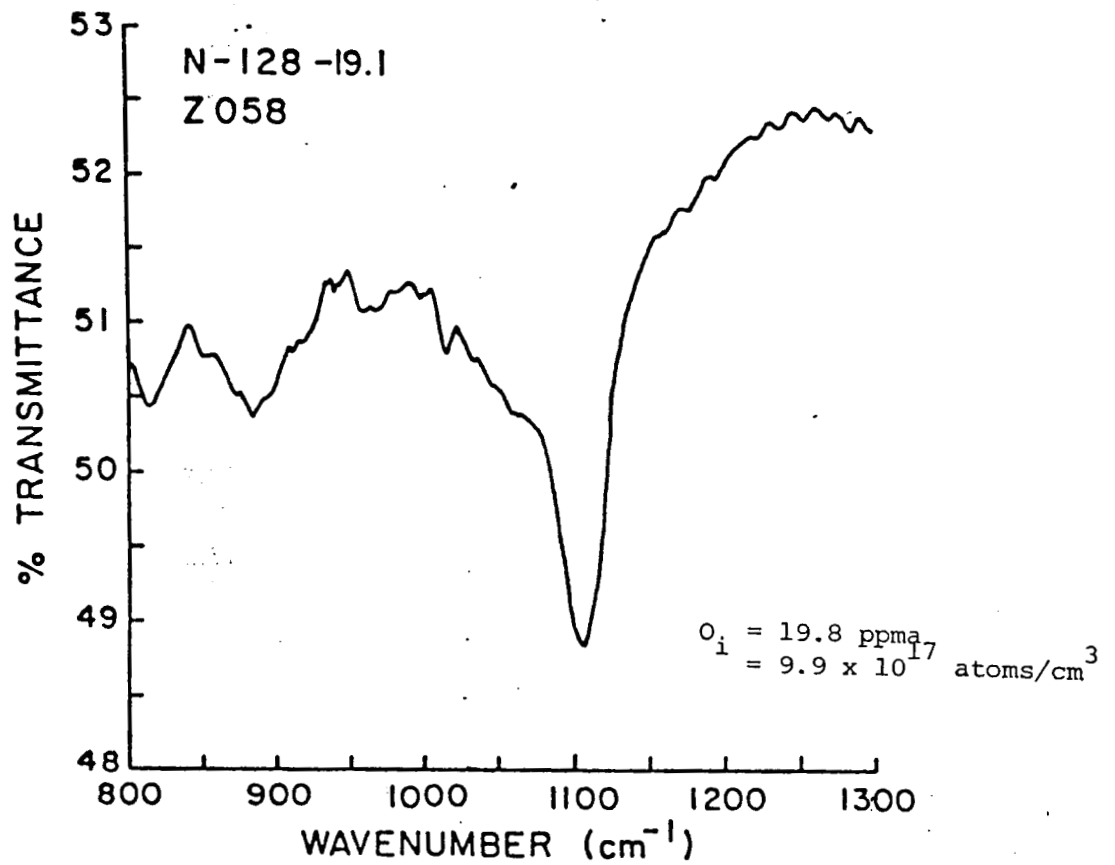
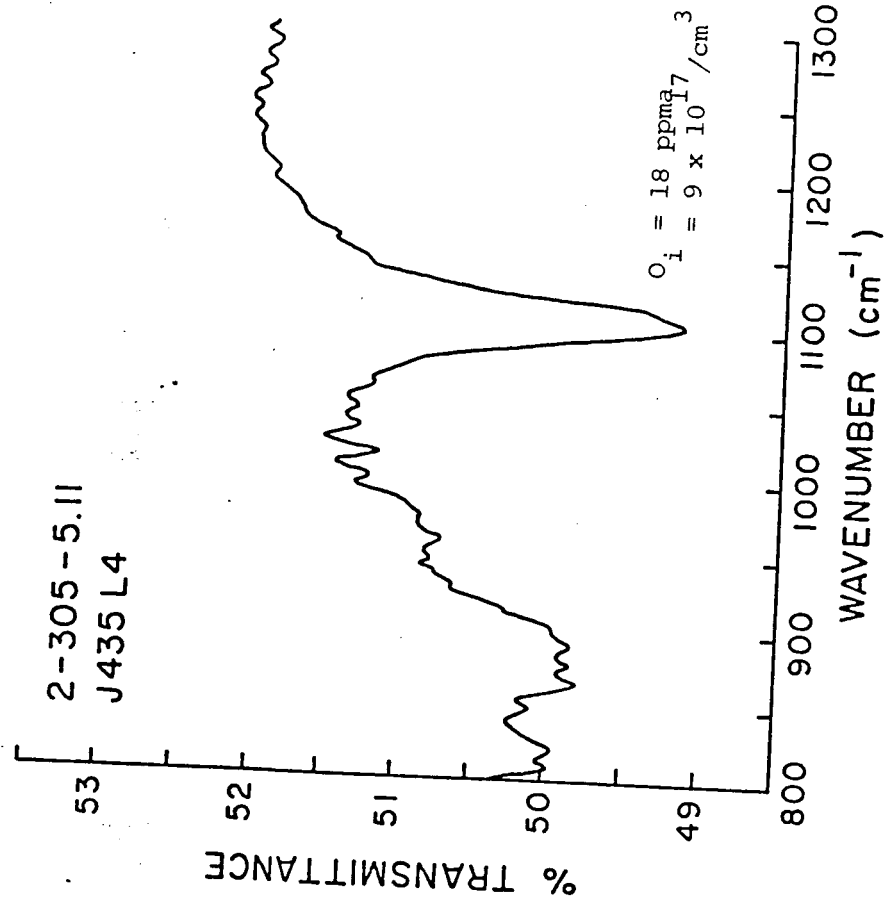
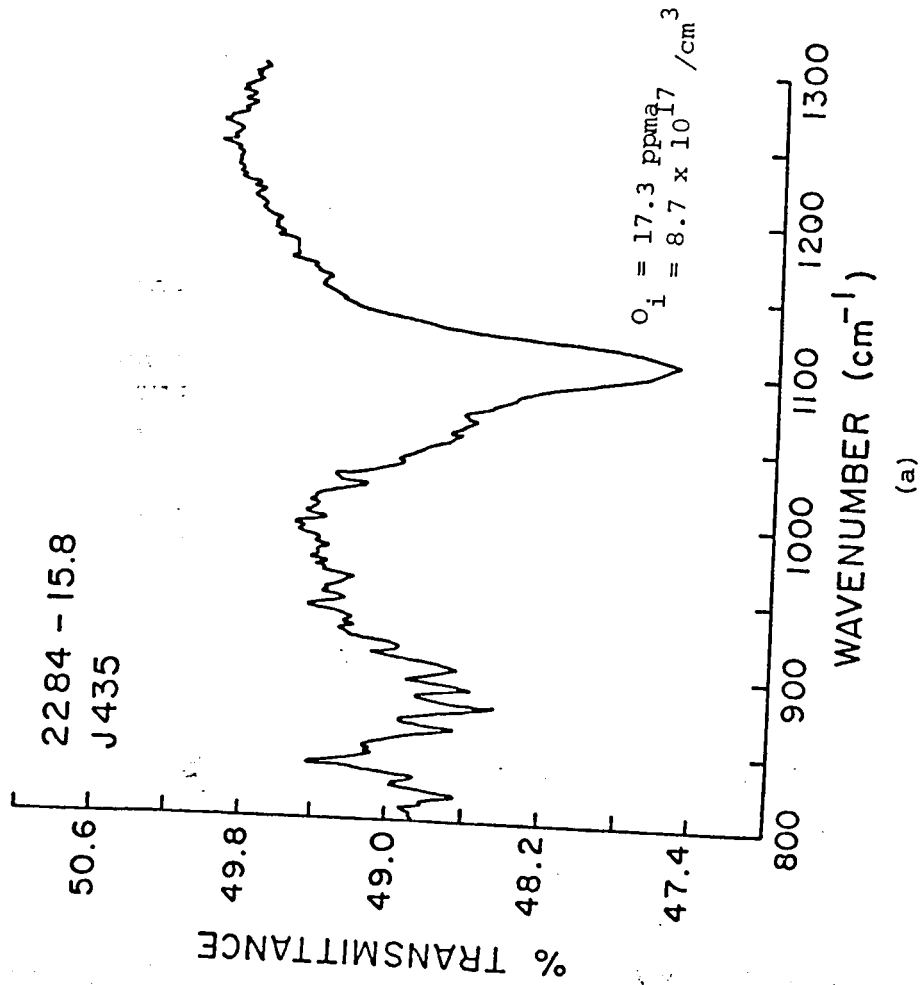


Figure 12: Intensity of the transmitted IR beam vs. wavenumber for Web sample N128-19.1 showing a distinct shoulder on the interstitial oxygen peak.



(a)

(b)

Figure 13: Intensity of transmitted IR beam vs. wavenumber for (a) Web sample 2284-15.8 showing the shoulder on the interstitial oxygen absorption peak and (b) Web sample 2-305-5.11 without the shoulder. Both samples were grown in the same growth configuration, J435. (1000 sacns)

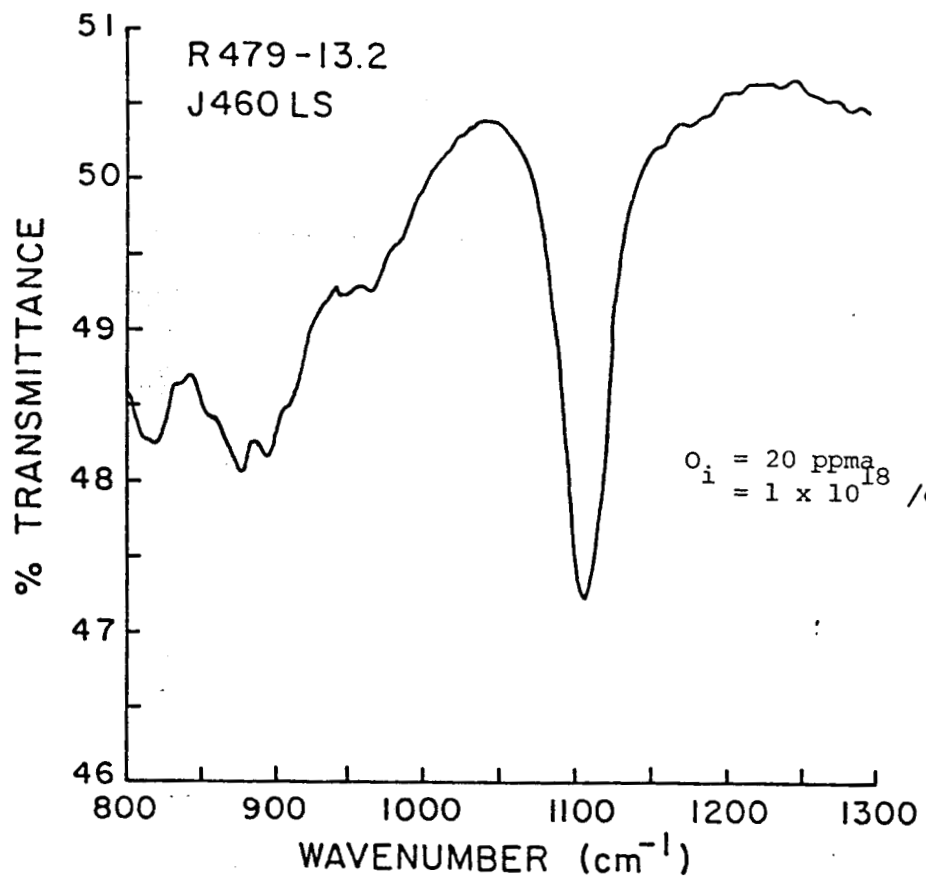


Figure 14: Intensity of transmitted IR beam vs. wavenumber for Web sample R479-13.2. (1000 scans)

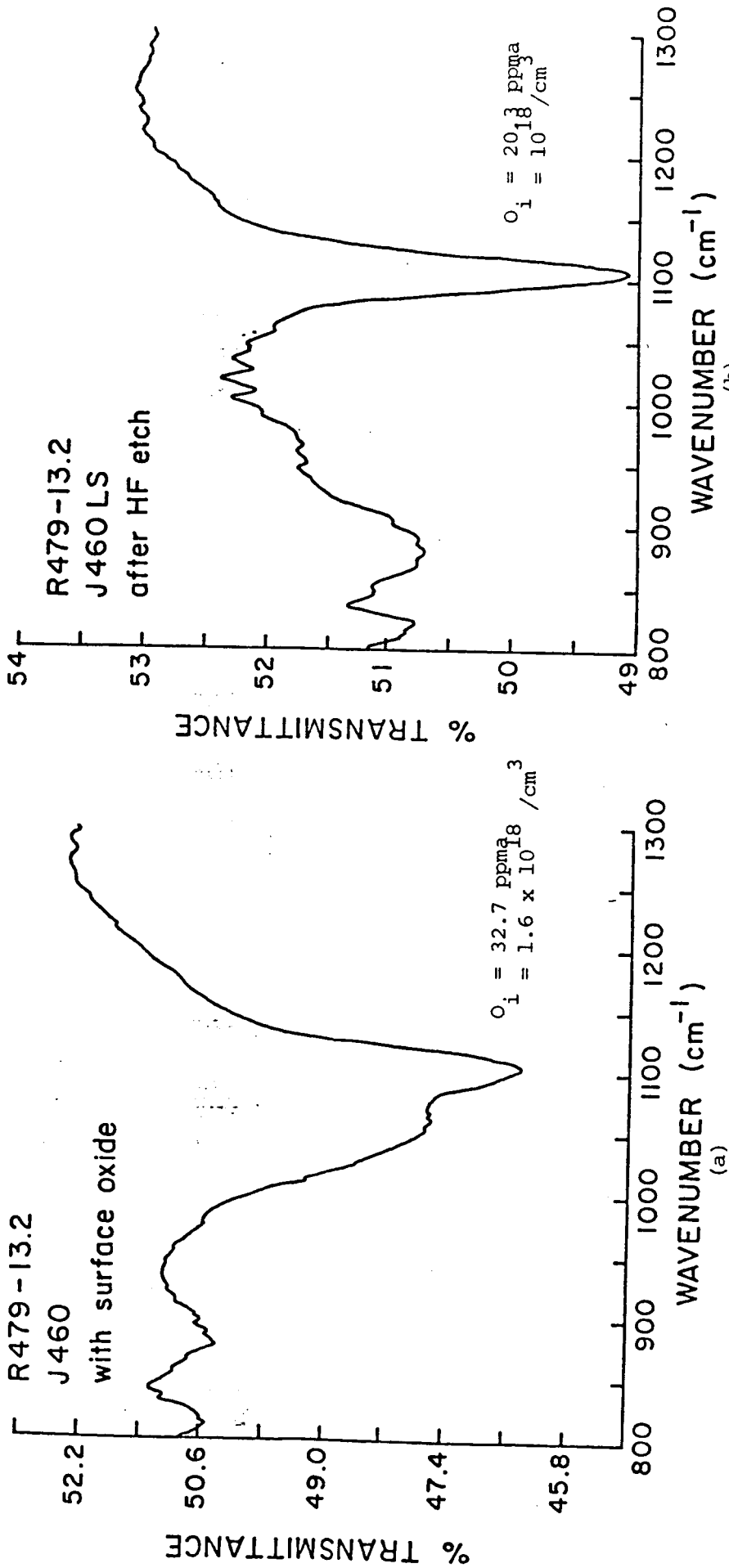


Figure 15: Intensity of the transmitted IR beam vs. wavenumber for Web sample R479-13.2, (a) before and (b) after an HF dip to remove the heavy surface oxide. The heavy oxide on the surface of this ribbon can be seen to make interpretation of the data very difficult.

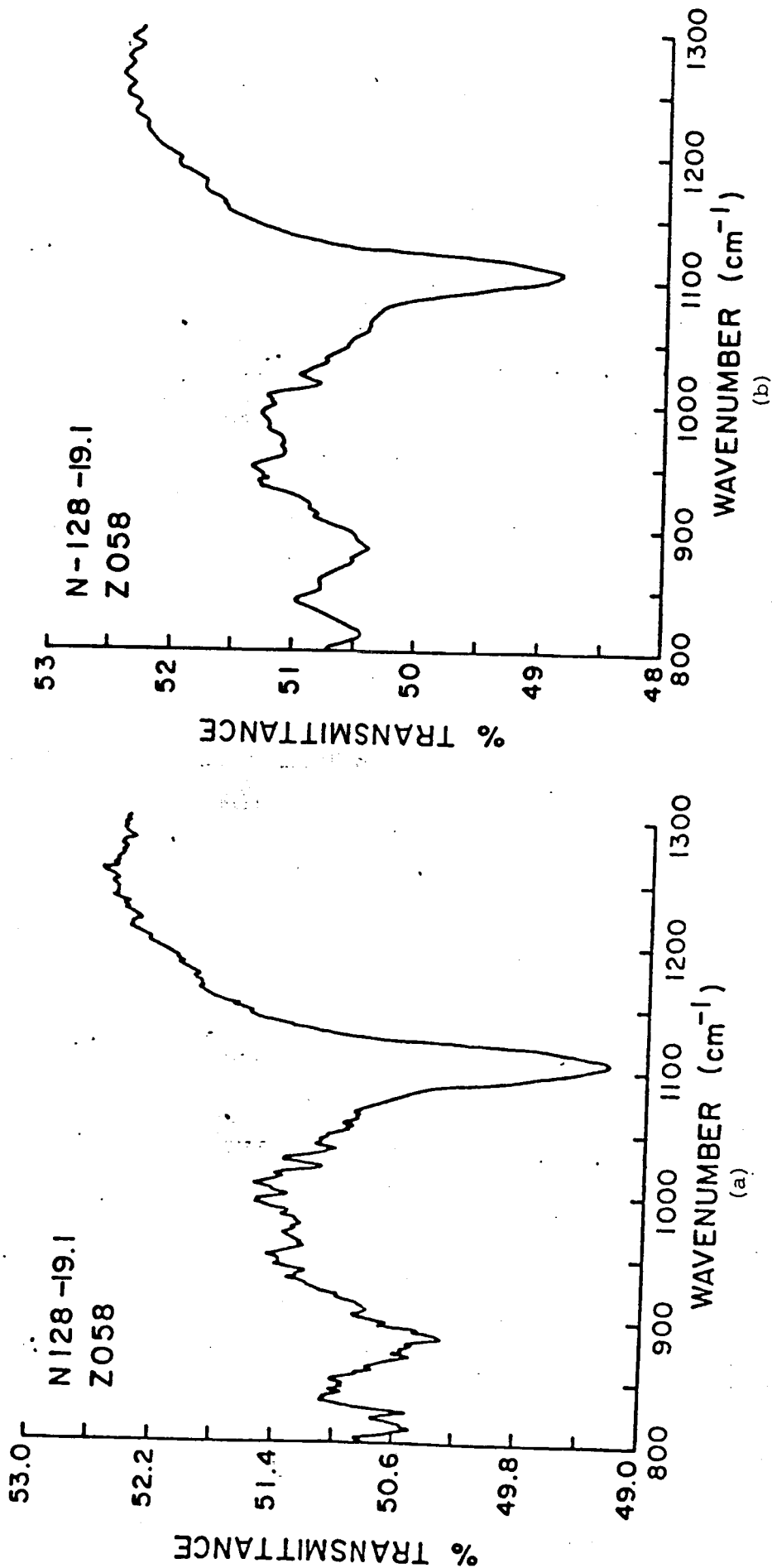


Figure 16: Intensity of the transmitted IR beam vs. wavenumber for two spots approximately 20 cm apart on the same sample, N128-19.1. One area of the ribbon shows little development of the shoulder on the interstitial oxygen peak, (a), while another area of the same ribbon shows the shoulder distinctly, (b).

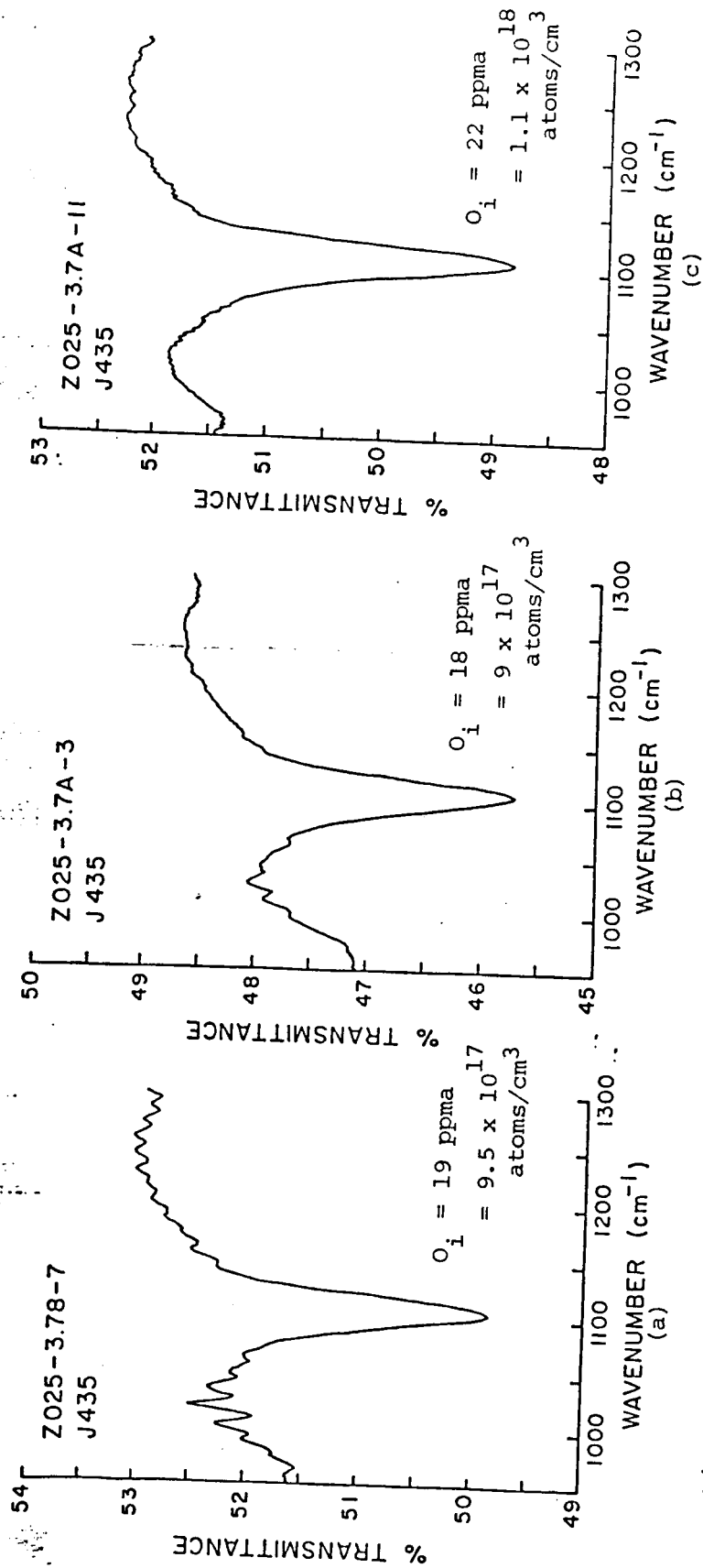


Figure 17: Intensity of the transmitted IR beam vs. wavenumber for three spots across the width of Web sample Z025-3.7A. There is a slight decrease in the width of the peak at the center of the ribbon, but there seems to be no significant trend.

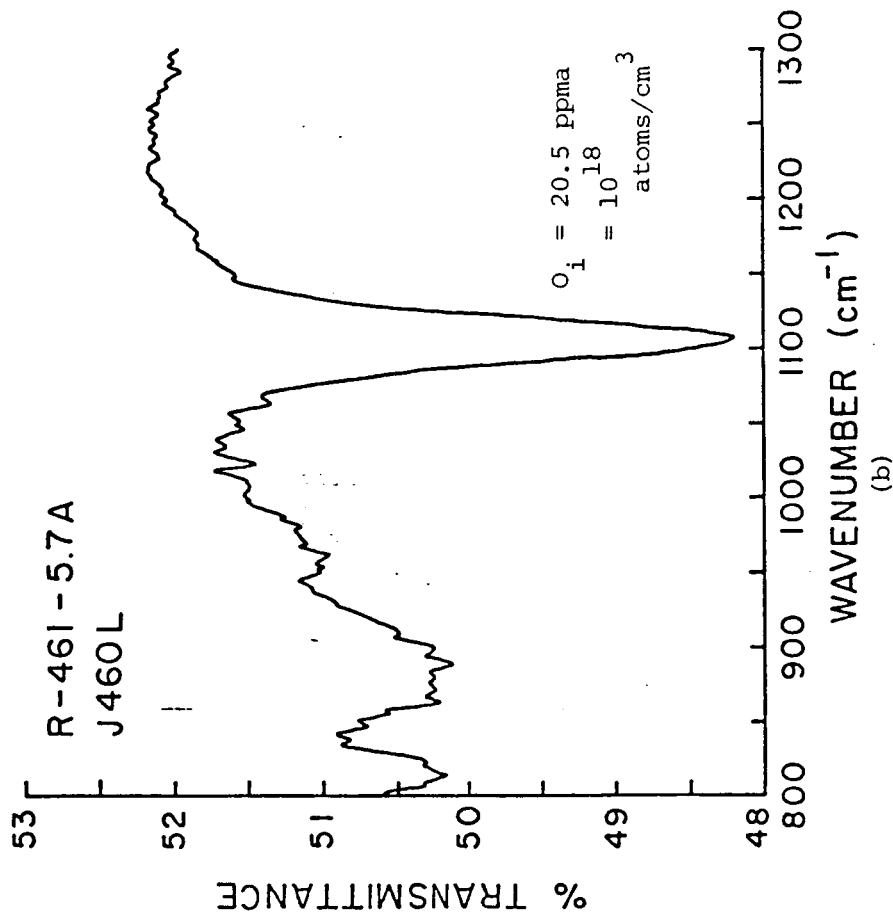
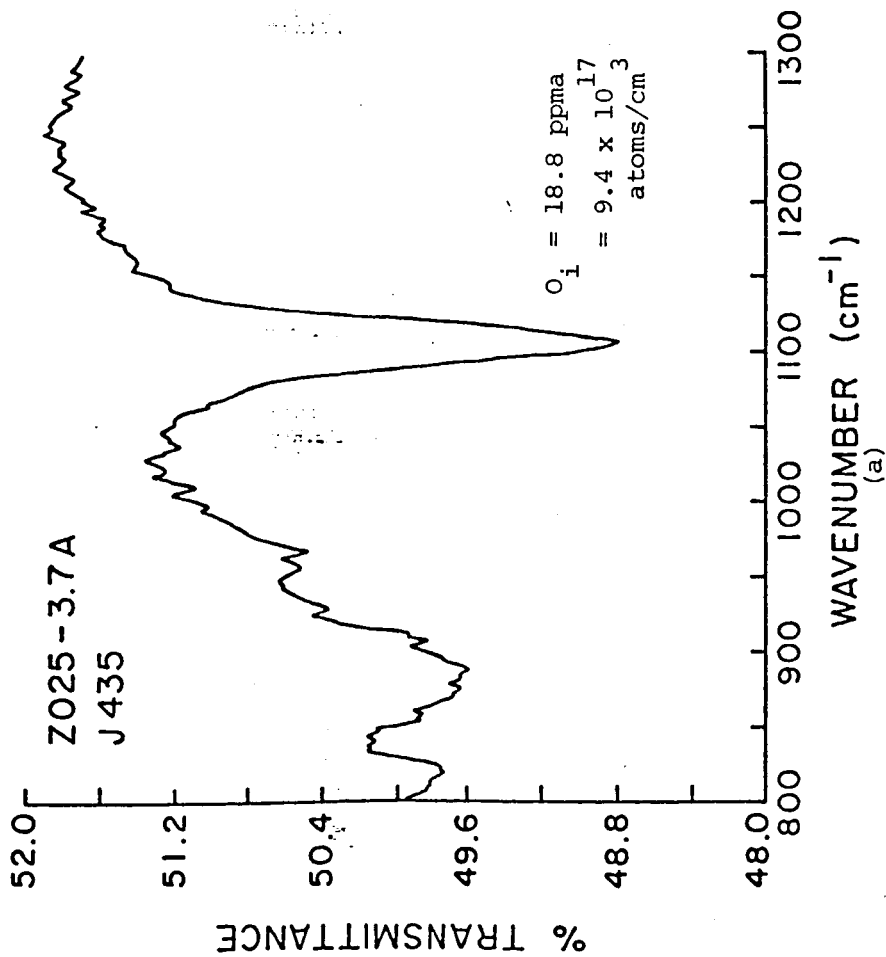


Figure 18: Intensity of the transmitted IR beam vs. wavenumber for Web samples with a known amount of stress. Sample (a), Z025-3.7A has a residual stress of 40 Mdyn/cm²; sample (b), R461-5.7A, has a residual stress of -3 Mdyn/cm². The FWHM for the sample with the greater amount of stress is greater than the FWHM for the sample with the lower amount of residual stress.

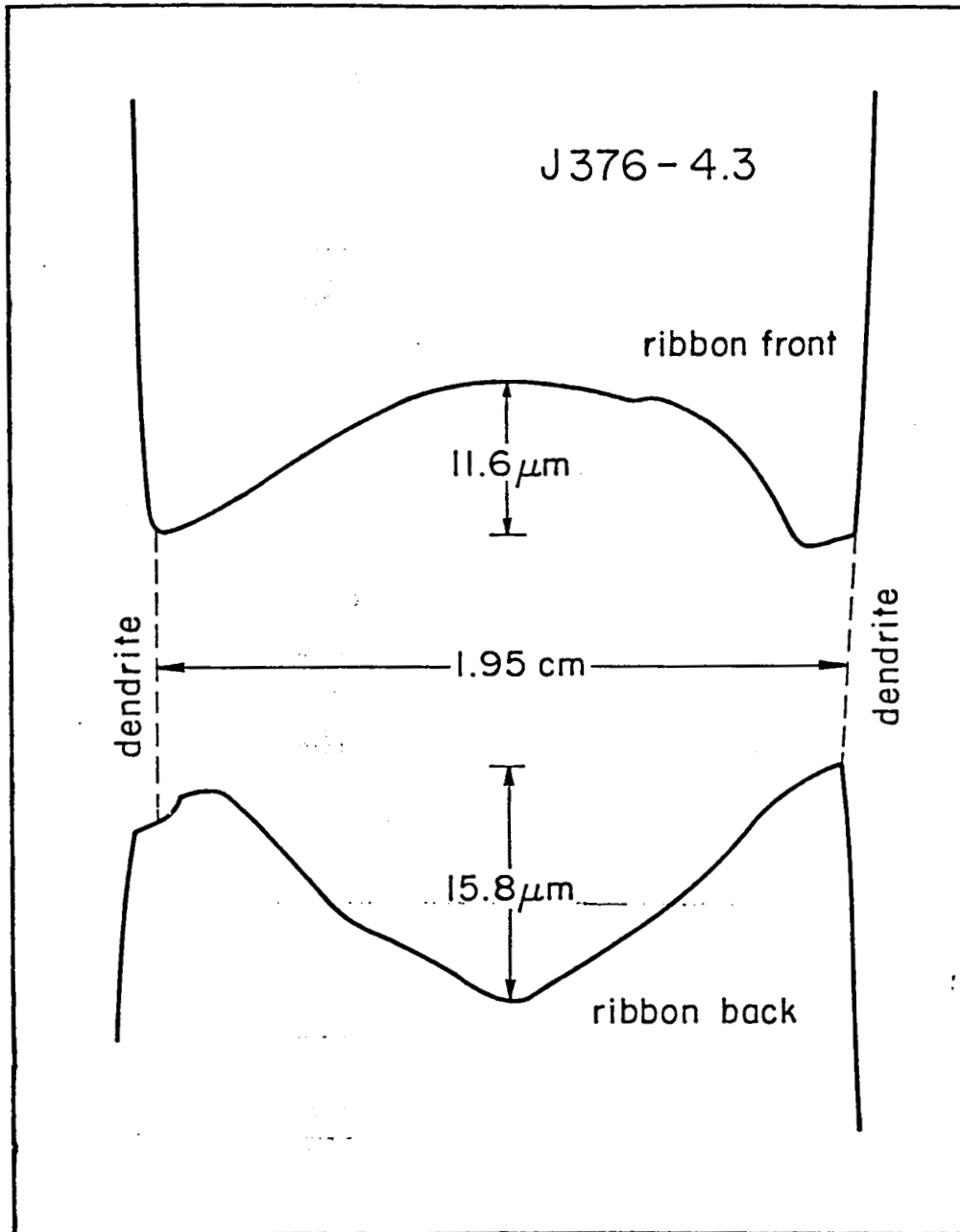


Figure 19: Surface profile of top and bottom of Web ample J376-4.3 showing a large variation in sample thickness from dendrite to dendrite. This ribbon was measured to be approximately 130 microns thick in the ribbon center.

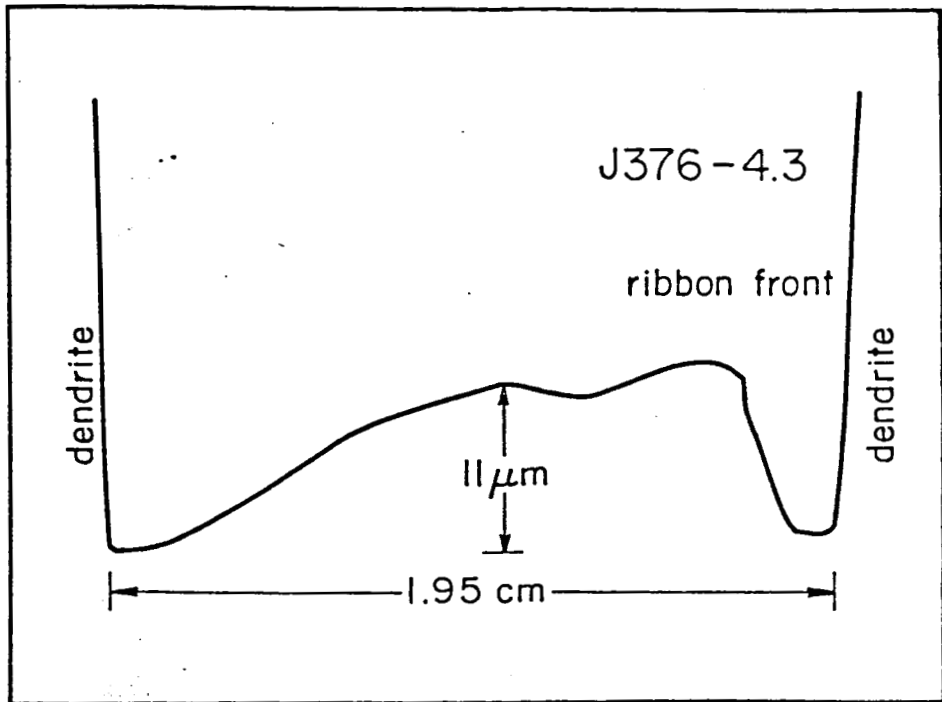


Figure 20: Surface profile of the front surface of the ribbon shown in Figure 18, but approximately 10 cm away from the previous profile. There is a significant change in the ribbon profile over this short distance.

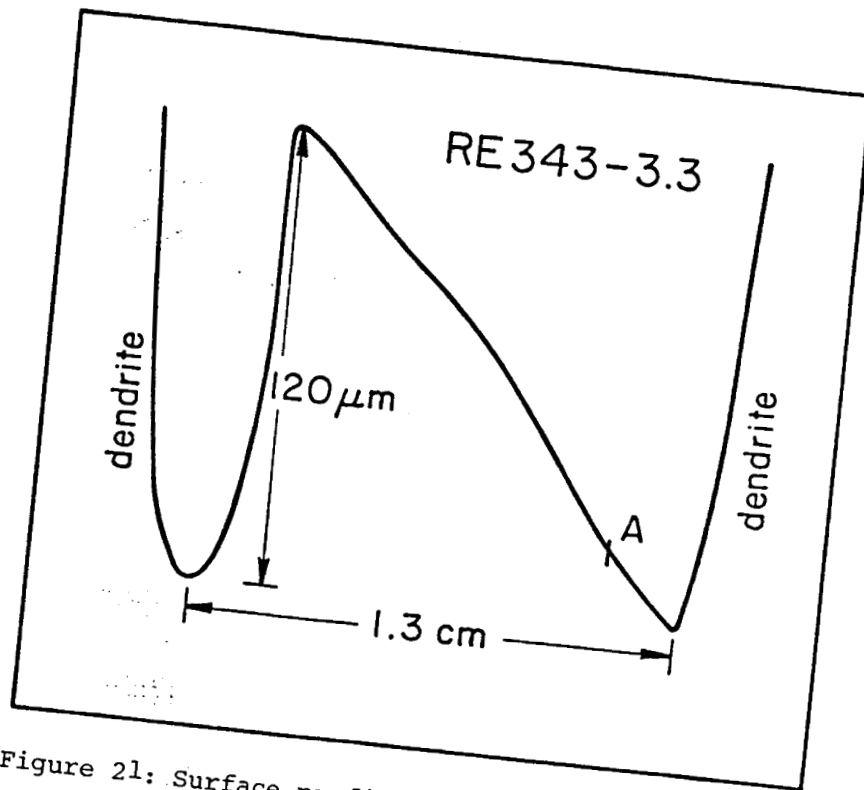


Figure 21: Surface profile of Web ribbon RE343-3.3 showing a 120 micron "hump" on the ribbon surface. This ribbon was measured to be approximately 120 microns thick in the ribbon center.

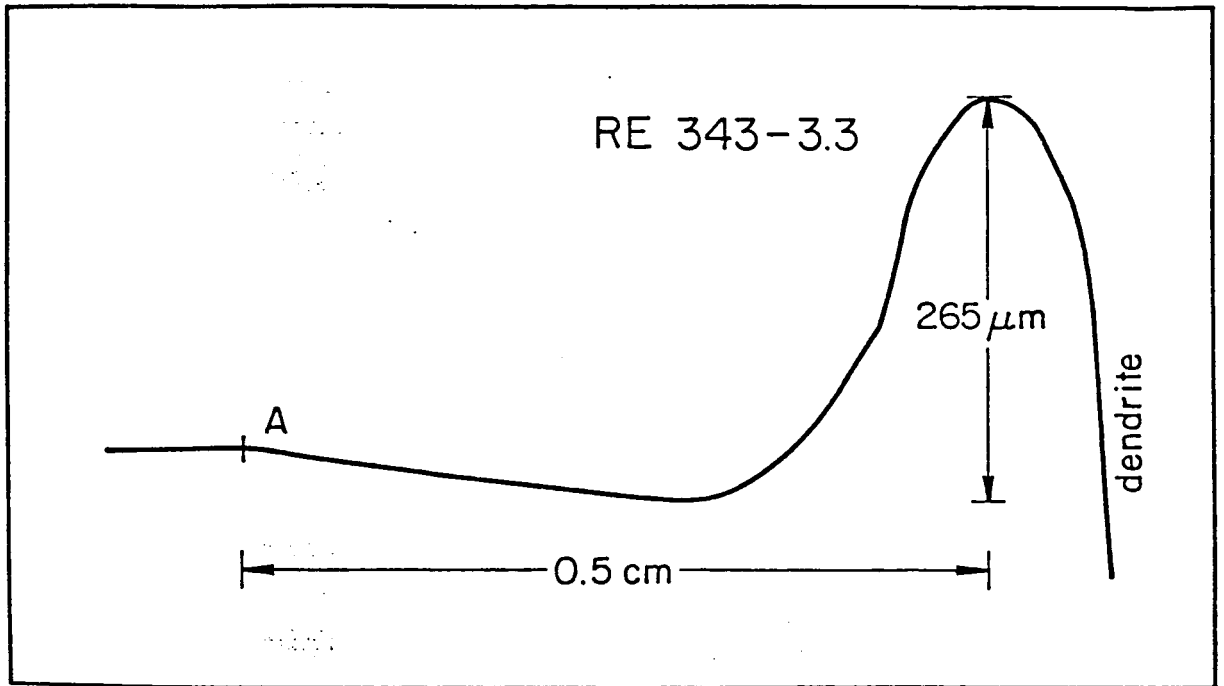


Figure 22: Expansion of the trace shown in Figure 20 for Web sample RE343-3.3 showing how the crystalline ribbon joins smoothly into the supporting dendrite.